







Inherited Grain-Size Distributions: Effect on Heavy-Mineral Assemblages in Modern and Ancient Sediments

Sarah Feil¹ , Hilmar von Eynatten¹, István Dunkl¹ , Jan Schönig¹ , and Nils Keno Lünsdorf¹ 

¹Department Sedimentology and Environmental Geology, Georg-August-Universität Göttingen, Geowissenschaftliches Zentrum, Göttingen, Germany

Special Section:

Controls and Biasing Factors in Sediment Generation, Routing, and Provenance: Models, Methods, and Case Studies

Key Points:

- Understanding factors that can modify a heavy-mineral assemblage is fundamental in provenance analysis
- Heavy minerals of two distinct sedimentary environments were analyzed and compared to their “ideal” hydrodynamically sorted compositions
- Several heavy-mineral species of modern and ancient settings were identified to be influenced by grain-size inheritance from the source

Correspondence to:

S. Feil,
sarah.feil@uni-goettingen.de

Citation:

Feil, S., von Eynatten, H., Dunkl, I., Schönig, J., & Lünsdorf, N. K. (2024). Inherited grain-size distributions: Effect on heavy-mineral assemblages in modern and ancient sediments. *Journal of Geophysical Research: Earth Surface*, 129, e2023JF007356. <https://doi.org/10.1029/2023JF007356>

Received 24 JUL 2023

Accepted 21 JAN 2024

Author Contributions:

Conceptualization: Hilmar von Eynatten

Data curation: Sarah Feil

Formal analysis: Sarah Feil

Methodology: Sarah Feil, Hilmar von Eynatten, Jan Schönig, Nils Keno Lünsdorf

Supervision: Hilmar von Eynatten

Writing – original draft: Sarah Feil

Writing – review & editing: Sarah Feil, Hilmar von Eynatten, István Dunkl, Jan Schönig, Nils Keno Lünsdorf

© 2024. The Authors.

This is an open access article under the terms of the [Creative Commons Attribution License](https://creativecommons.org/licenses/by/4.0/), which permits use, distribution and reproduction in any medium, provided the original work is properly cited.

Abstract Heavy-mineral suites are used widely in sandstone provenance and are key when connecting source and sink. When characterizing provenance related signatures, it is essential to understand the different factors that may influence a particular heavy-mineral assemblage for example, chemical weathering or diagenetic processes. Hydrodynamics, causing size-density sorting, exert major control on the distribution of heavy minerals. Here, we highlight the effect of grain-size inheritance, essentially the absence of certain grain sizes within a specific heavy-mineral species, on two distinct types of sediments. Modern deposits from a high-energy beach in NW Denmark give an analog for heavily reworked sediment, primarily controlled by hydrodynamic processes. In contrast, three Palaeogene turbidite successions in the Eastern Alps were sampled, presenting a more complex history that includes diagenesis. All samples were processed for their heavy-mineral compositions using Raman spectroscopy, and several techniques applied to determine the effect of grain-size inheritance. Results show that (a) even within the hydrodynamically well-sorted beach and placer deposits, evidence of grain-size inheritance is apparent, and (b) turbidites of variable heavy-mineral composition show strong effects of grain-size inheritance for several mineral species. Moreover, considerable intersample contrasts within single turbidite beds are observed. We enforce the importance of understanding grain-size inheritance, as well as other processes effecting size-density relations in clastic sediment that go well beyond purely hydrodynamic control of intrasample heavy-mineral variability.

Plain Language Summary Heavy minerals are commonly found within sediments and sedimentary rocks and can tell us from which source regions the sediment may have originated. However, it is important to understand that the type, size, and abundance of particular heavy minerals can change depending on factors such as environmental conditions. The size, shape, and density of the heavy minerals also limits when and where they will settle and/or stay. A lack of big or small grains of a particular heavy mineral in the source rocks dictates the size of the minerals deposited; this is known as grain-size inheritance. Using both ancient and modern sediment, we are looking for traces of grain-size inheritance. Surprisingly, in all samples investigated we noted effects of grain-size inheritance, for different heavy-mineral types. The modern beach sediments, as expected, show more impact of hydraulic processes, but inherited grain sizes are still apparent. Within the ancient examples, grain-size inheritance is more obvious, with further variations even observed between samples collected from the same area. Having identified this control on grain size, we can highlight the importance of understanding this effect when analyzing clastic sediments.

1. Introduction

When attempting to reconstruct sediment history in provenance studies, the heavy-mineral assemblage is an essential tool for connecting source and sink. Heavy minerals are diverse, widely available in crystalline source rocks in addition to their eroded siliciclastic sediments, and require a relatively simple technique to extract and analyze (Mange & Maurer, 1992). The array of heavy minerals presented (usually given as those with a density $>2.85\text{--}2.9\text{ g/cm}^3$) is related to those available in the parent rock, meaning direct comparisons can be made and quantified when identifying source regions (Mange & Wright, 2007; von Eynatten & Dunkl, 2012). However, during the sedimentary cycle these heavy-mineral assemblages undergo various processes that can substantially alter their relative abundances (Garzanti & Andò, 2019; Morton, 1985; Morton & Hallsworth, 1999). Thus, when applying heavy-mineral analysis in provenance studies, it is essential to disentangle non-source-related modifications from source-related signatures.

Before weathering and erosion begins to modify the heavy-mineral assemblage, the nature of the source rock itself defines what may be called the “initial or potential heavy-mineral spectrum.” Typically, these heavy minerals have specific grain-size distributions, for instance, garnet is relatively coarse in eclogites or paragneisses, while zircon is relatively fine in most igneous and metamorphic rocks. This implies that heavy minerals do not have the same grain-size distribution when entering the sedimentary cycle. This may pose significant constraints on the grain-size distribution of heavy minerals observed in the final sediment. This effect is referred to in literature as grain-size inheritance (Mange-Rajetzky, 1983; Morton & Hallsworth, 1999; Krippner et al., 2015, 2016; van Aniel, 1950; von Eynatten & Dunkl, 2012).

There are four main factors controlling the heavy-mineral assemblage within the sedimentary cycle (Mange & Maurer, 1992; van Aniel, 1959; Weltje & von Eynatten, 2004). First, weathering of the parent rock in the critical zone determines the assemblage of mineral grains delivered to the transport system. At this stage, depending on the climatic conditions and relief in the source area, chemical weathering may cause selective mineral dissolution (Andò et al., 2012; Morton & Johnsson, 1993; Velbel, 2007). Next, during transport grains undergo mechanical abrasion processes leading to grain size reduction and changes in relative abundances, particularly applicable to more mechanically unstable minerals. However, these physical processes are found to have little significance on the resulting heavy-mineral assemblage (Morton & Smale, 1990; van Aniel, 1959). In addition, whilst minerals are intermittently stored on sandbars and flood plains, further chemical modification by weathering can take place before remobilization and transportation downstream (Morton & Johnsson, 1993). A major control, and thus highly relevant for this study, are the hydrodynamic processes effecting grain distributions during both transport and deposition. Selective grain sorting in this part of the sedimentary cycle causes differentiation based on grain size, density, and shape. It defines what and when grains will be deposited based on the hydraulic conditions present, that is, the heavy-mineral spectrum depends on the grain-size range considered (Garzanti et al., 2008, 2009). In theory, the distribution of heavy minerals within a sample can be modeled based on these physical hydrodynamic principles if required variables (e.g., grain size, sorting, and bulk composition) are known; such approaches are applied in provenance analysis to predict mineral distributions in non-studied grain-size fractions (Resentini et al., 2013). Finally, post deposition of a sediment, diagenetic processes during burial directly affects less stable minerals by intrastratal solution, that is, they become selectively depleted (Andò et al., 2012; Garzanti et al., 2018; Morton & Hallsworth, 1999; Turner & Morton, 2007).

In order to evaluate the effects of grain-size inheritance we applied multi-grain-size-window heavy-mineral analysis to modern beach placer and ancient turbidite deposits. A beach placer is a detrital deposit of concentrated higher density minerals in a coastal setting that can be of high economic value (Garnett & Bassett, 2005). Considering hydrodynamics, beach placers are typically sediments that have experienced high transport energy at the shoreline, and can form over long periods of time or during a single storm event (Hou et al., 2017). Thus, one expects other controls, as mentioned previously, to have little to no impact on these deposits. In contrast, turbidites present more of an unknown. Turbidite deposits are a vertical sequence of sedimentary structures showing a “rhythmic building pattern” (Bouma, 1962, 1964). Few studies have endeavored to constrain the variation in heavy-mineral abundance resulting from changes in flow parameters that effect settling velocities throughout a single turbidite sequence (Komar, 1991; Norman, 1969; Walker, 1965). Hence, to attain a greater understanding of grain-size inheritance, we test correlations between hydrodynamic sorting models and the observed examples from nature, both ancient and modern. We show that grain-size inheritance has a major control on the grain-size distributions of individual heavy-mineral species within all samples.

2. The Hydrodynamic Control on a Settling Grain

The difference in density, size, and shape of minerals within clastic water-laid sediments plays a major role in their behavior as they are entrained, transported downstream, and deposited. Thus, the grain-size distribution of light and heavy minerals varies substantially, with proportions of heavier minerals tending to contribute more toward finer grain sizes, and their counterpart toward the coarser end. The forces in play causing this phenomenon have been extensively studied for over a century (e.g., Rubey, 1933a, 1933b; Udden, 1914). Comprehensive reviews have been provided by Komar (2007) and Garzanti et al. (2008). The latter authors highlight that settling equivalence (i.e., grains exhibiting similar settling velocities as largely controlled by their sizes and densities) is the dominant cause for size-density sorting in clastic sediments, typically accounting for approx. 90% of intrasample variability, while other effects and causes are considered subordinate.

2.1. Sediment Sorting Processes

The settling velocity of a spherical grain in a fluid depends on the contrasting effects of gravitation and drag resistance. For fine-grained materials (i.e., silt) settling velocity is mostly controlled by fluid viscosity (Stokes' law) while for very coarse-grained materials (gravel) settling is mostly controlled by drag resistance resulting from fluid turbulence (Impact law). For materials in between (i.e., sand), combined effects are acting on the settling behavior of sand grains with very-fine sand ($\phi > 3.5$) approximating largely Stokes' law and very-coarse sand to granules ($\phi < -1$) approximating the Impact law. This transitional settling behavior is best approximated by Cheng's formula (Cheng, 1997; Garzanti et al., 2008).

Garzanti et al. (2008) introduced the "size shift" based on the principle of settling equivalence, which is noted as the difference in diameter (in phi-units) between two mineral species experiencing similar settling velocity, commonly a heavy mineral and quartz:

$$SS_m = \log_2(D_q) - \log_2(D_m) \quad (1a)$$

where SS_m is the size shift of mineral m , D_q , and D_m are the diameter (in millimeters) of quartz and mineral m , respectively. The transformation between millimeters and phi is defined as:

$$\Phi = -\log_2(D) \quad (1b)$$

The formulas for calculating the size shifts for silt-, gravel-, and sand-sized water-laid sediments follow the three cases described above for settling velocities. These are given below:

$$SS_{st} = \frac{\log_2\left(\frac{\Delta_m}{\Delta_q}\right)}{2} \quad (2)$$

$$SS_{gl} = \log_2\left(\frac{\Delta_m}{\Delta_q}\right) \quad (3)$$

$$SS_{sd} = \log_2\left(\frac{\Delta_m}{\Delta_q}\right) - \frac{3}{2} \log_2\left(\frac{\Xi_m}{\Xi_q}\right) \quad (4a)$$

Ξ_m is defined as:

$$\Xi_m = \frac{v}{\eta} + \left(\left(\frac{v}{\eta} \right)^2 + 48 \left(g \cdot \frac{\Delta_m}{\eta^2} \right)^{\frac{2}{3}} \right)^{\frac{1}{2}} \quad (4b)$$

where SS_{st} , SS_{gl} , and SS_{sd} is the size shift of a silt-, gravel-, and sand-sized mineral, Δ_m and Δ_q is the submerged density of mineral m and quartz (density difference between mineral and fluid), v is settling velocity, η is the dynamic fluid viscosity (0.0105 g/cm s for seawater) and g is gravity. Calculated size shifts are thus increased by factor 2 for gravel compared to silt and intermediate for sand (about factor 1.7 compared to silt according to Garzanti et al., 2008).

Beyond grain size and density, the sorting of detrital grains may be influenced by fluid density and grain shape, in addition to hydrodynamic processes other than settling. Fluid density is negligible when considering water-laid sediments only (Garzanti et al., 2008). However, in case of higher-density fluids (e.g., turbidity currents), fluid density may become relevant (see below). Grain shape is quite relevant for extreme cases such as platy micas (size shift of up to ~0.4 for Corey Shape Factor = 0.1) but is of minor relevance for quartz and most other natural grains (Garzanti et al., 2008). Moreover, the global availability of minerals via the entire relevant grain-size range may not exist for specific source regions (i.e., inherited grain-size distributions from the sediment sources, see below).

Hydrodynamic processes, other than settling, that potentially affect size-density sorting include selective re-entrainment (e.g., McIntyre, 1959; Slingerland, 1977), and hindered settling (e.g., Richardson & Zaki, 1954). All grains undergo grain entrainment during the sedimentary cycle. Re-entrainment occurs when grains previously deposited, for example, in a riverbed or beach environment, are selectively picked up into the flow due to their physical characteristics. Heavy-mineral sorting through selective re-entrainment has been characterized in

several studies. McIntyre (1959) observed that quartz grain sizes in beach sand were too small when in comparison to their hydraulically equivalent heavy minerals. He suggested this observation is a result of coarse quartz grains being preferentially re-entrained and transported away. Smaller heavy minerals are less easily re-entrained due to them being shielded from the current by their hydraulically equivalent, larger, light mineral. Further works by Slingerland (1977, 1984) and Komar and Wang (1984) attempted to quantify this effect, with special reference to the formation of placer deposits. In essence, preferential entrainment of coarser lower density grains (typically quartz) reduces the size shift within the remaining (placer) deposit. Garzanti et al. (2009) found that this effect is rather small within the analyzed individual samples and concluded that intrasample variability is governed by settling equivalence in sorted sediments in any type of depositional environment.

Most studies on the controls on sediment and heavy-mineral sorting focus on grains deposited or concentrated by running water in environments such as rivers or beaches. However, turbidites are hydrodynamically distinct, form a significant part of siliciclastic sediments on Earth, and serve as most distal archives in sediment routing systems (Bouma, 1964). They are hydrodynamically distinct for a few reasons including size, speed, and density of the flows (e.g., Talling et al., 2012). The settling velocity of detrital grains in suspension can be reduced by high sediment concentrations. This is known as hindered settling, where grain-grain interactions increase drag resistance and thus slow down settling rates (Richardson & Zaki, 1954), and the proportions of heavy and light minerals being deposited (Slingerland & Smith, 1986). The hindered settling effect was found to become relevant when sediment volume concentrations reach 10% and increasingly important above it (Bagnold, 1954; Richardson & Zaki, 1954). A recent study suggests a modified hindered settling equation and emphasizes that the hindered settling effect increases with decreasing grain size, that is, even a few percent of fine-grained sediment volume concentrations can substantially influence the settling behavior (Baas et al., 2022). For instance, a 50% reduction in settling rate is found for a 25- μm -sized silt grain at 13% sediment concentration, while 25% sediment concentration are required to have the same effect on a 4,000- μm -sized pebble. If the impact of hindered settling, which is a known occurrence within high-density turbidity flows, is capable to influence hydraulic equivalence, this could have a significant impact on heavy-mineral assemblages (in case of sediment volume concentrations $\geq 10\%$; Talling et al., 2012).

So far, only few studies have investigated heavy-mineral fractionation within turbidites. Norman (1969) used a kind of normalized grain abundances to understand the changes within an early Cenozoic (likely Eocene) turbidite located east of Ankara, Turkey. He concluded that heavy-mineral distributions have the smallest vertical variation at and just above the central part of the bed, with distal sections of the turbidite having more uniform vertical distributions; unfortunately no sedimentological characterization is available. Just a handful of studies have attempted to deduce the hydrodynamic conditions for grain entrainment and deposition during turbidite formation (e.g., Allen, 1982; Komar, 1985; van Tassel, 1981; Walker, 1965). Komar (1985), although less heavy-mineral specific, produced a detailed overview of the hydraulic conditions present during the deposition of a turbidite sequence. They used both the grain-suspension criterion (using measured settling velocity values and grain size), and the relationship between sedimentary structures and flow intensity, to determine the flow conditions during deposition. Flow conditions included the type of flow, flow velocity, and bottom stresses, and these were found for different stages within the Bouma sequence. Pyles et al. (2013) performed physical experiments at the lab-scale with low-density turbidity currents composed of artificial particle mixtures and found that while being spatially fractionated, the samples at any one location were in hydrodynamic equivalence.

2.2. Grain-Size Inheritance

Dissimilarities observed between estimated heavy-mineral grain-size distributions, determined by settling equivalent equations, and the actual observations in natural samples can be attributed to grain-size inheritance. Essentially, if only certain mineral grain sizes are available in the parent rock, even after grains are in hydraulic equivalence, these minerals will not be necessarily present in the deposited material. Interpretations of grain-size inheritance date back to Rittenhouse (1943), van Andel (1950), and Briggs (1965). Rittenhouse (1943) found the lowest hydraulic ratios in the coarser grain sizes for sands of the Rio Grande, emphasizing that a deficiency of larger-sized heavy minerals in the source would lead to this reduced availability. Likewise, Briggs (1965) recognized an anomaly of coarse magnetite and ilmenite grains within Palaeocene to Eocene sediments, linking them to a group of Precambrian granites from which these grains were likely to have originated. Examining sediment maturity in coastal and river settings of Baixada de Jacarepaguá (Brazil) gave insights into how inherited

Table 1
An Overview of Modern and Ancient Samples Analyzed Including Their Locations

| Sample | Latitude | Longitude | Elevation (m) | Locality | Deposit |
|---------------------|------------|------------|---------------|-------------------|---------------------|
| EY-62 (01, 02, 03) | N 56.96508 | E 8.38598 | 0 | Vorupør, Denmark | Placer (modern) |
| SF-1-2 (A, B, D, F) | N 48.34805 | E 16.25737 | 237 | Höfleln, Austria | Turbidite (ancient) |
| SF-1-6 (A, B) | N 47.90169 | E 13.01821 | 501 | Strubach, Austria | Turbidite (ancient) |
| SF-1-8 (A, B) | N 47.66212 | E 14.85054 | 691 | Gamsbach, Austria | Turbidite (ancient) |

distributions can change over a long distance (Savage et al., 1988). The river sediments display an unusual size-density relationship with no correlation between density and mean grain size. In contrast, the beach sands exhibit a distinct relationship. This is attributed to their longer travel distance and resulting attainment of hydraulic equilibrium over time (Savage et al., 1988; see Figure 5 in Morton & Hallsworth, 1999 for heavy-mineral grain-size distributions). Contrasting heavy-mineral abundances within varying grain-size fractions compared to hydrodynamically expected trends are similarly reflected in stream sediments from the Tauern Window, Eastern Alps (Krippner et al., 2015) and the Western Gneiss Region, SW Norway (Krippner et al., 2016). In the former case, garnet as well as amphibole are enriched in the coarser fractions while apatite, epidote, and staurolite are enriched in finer fractions. In the Norway example, higher concentrations of garnet in coarser grain-size fractions (125–500 μm) contrast with high concentrations of pyroxene and amphibole in the 63–125 μm fraction. Such contrasts can be extreme in even smaller-sized catchments (see Figure 4c in Schönig et al., 2023). Although related to relatively small-scale catchments, these studies outline the effect of grain-size inheritance and a lack of mineral hydraulic equivalence, at least for proximal depositional settings.

Grain-size inheritance can have serious effects when investigating specific single-grain based provenance signatures such as mineral chemistry or U-Pb ages, depending on the grain-size fraction(s) analyzed. Von Eynatten & Dunkl (2012) compiled data on modern detrital tourmaline (Cheyenne River and tributaries, SD, USA) from Viator (2003), finding that finer grain sizes (<250 μm) contain mostly metamorphic tourmaline, compared to high proportions of granitic tourmaline seen in the coarser sediments. Similarly, garnet geochemistry, commonly used as a provenance indicator, may strongly depend on grain size (Krippner et al., 2015, 2016; Schönig et al., 2021). While garnet sourced from high-grade metamorphic rocks is commonly enriched in the coarser grain-size fractions, this trend can be reversed in cases where lower-grade micaschists containing coarse-grained garnet contribute to the sediment factory (cf. Figures 1 and 3 of Schönig et al., 2021). Furthermore, it has been observed that the number of coesite inclusions in ultrahigh-pressure detrital garnet influences the disintegration process, that is, garnet grains with a higher number of coesite inclusions (felsic sources) extensively disintegrate into smaller fragments compared to mafic garnets which have a lower number of coesite inclusions (Schönig et al., 2021). Lawrence et al. (2011) and Augustsson et al. (2018) provide two examples highlighting the effect of size fractionation on zircon age populations. Both these studies determine that specific zircon grain sizes preferentially convey certain ages that may not be present (or at least less frequently) in other size-groups. This holds at the basin scale with, for instance, overall older ages obtained from smaller zircons in both studies (modern Amazonas drainage basin, Lower Triassic Central European Basin, respectively), as well as at the scale of individual bedforms such as subaquatic dunes (Lawrence et al., 2011; von Eynatten & Dunkl, 2012). It is worth noting, the tendency of detrital minerals to preserve multiple geochronological domains (e.g., age zonation) within the same grain (Zimmermann et al., 2018) may qualitatively reduce the effect of grain size bias.

3. Materials and Methods

3.1. Sample Collection

All samples have been alphabetically or numerically named from the base upwards (i.e., “A” or “01” would be the lowermost sample), Table 1 contains an overview of all samples and their locations.

The modern samples were collected from a beach 2.5 km north of Vorupør, located in Northwest Denmark (Figure 1a; location EY-62). Geologically, this area lies within the “flyvesand,” that is wind-blown sand that formed thick Holocene-age aeolian sand deposits (Clemmensen et al., 2001). However, the creation of this placer deposit is a result of wave action following coastal erosion and reworking at the foreshore and shoreface,

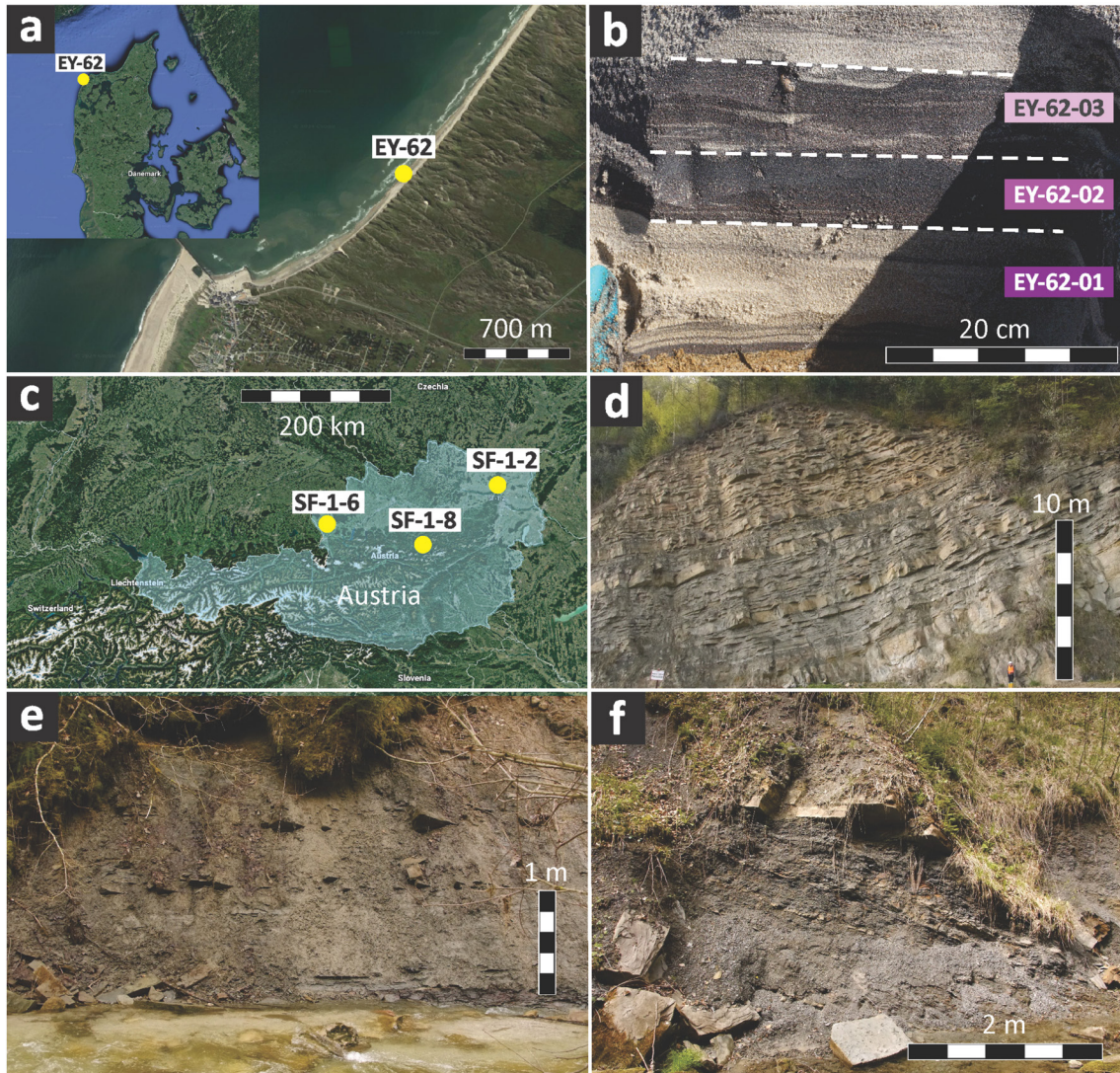


Figure 1. Sample locations and field photos. (a) Sample locality of modern beach placer deposit (EY-62), coastal town of Vorupør (NW Denmark) visible in the bottom left corner (image from Google Earth, 2023). (b) Vertical cross-section of beach deposit, with marked distinctions between each layer sampled. (c) Sample localities for the ancient turbidite deposits within the Eastern Alps (SF-1-2, 6, 8; image from Google Earth, 2023). (d) Rock face displaying turbidite strata from the Höflein quarry locality (SF-1-2). (e) Heavily eroded Strubach Section outcrop, sample collected from visible rock ledges (SF-1-6). (f) Eroded and vegetated Gamsbach outcrop, sample collected from strata in the bottom right corner of image (SF-1-8).

rather than wind. A vertical section of approx. 25 cm displays three distinct layers: (01) light-colored “normal” background beach sand, (02) dark-colored heavy-mineral-rich placer deposit, and (03) a layer with intermediate composition (Figure 1b). Approximately 400–500 g of sand was sampled for each layer.

Turbidite deposits were sampled at three locations in the Eastern Alps (Figure 1c), at each location samples were taken from different layers within a single sandstone bed. Location SF-1-2 is found at the “Strombauamt” quarry in the town of Höflein, situated just west of Vienna. On the eastern section of the Rhenodanubian Flysch zone, this sample was taken from the Greifenstein Formation, containing glauconite-rich, weathered sandstones, conglomerates, and thick-bedded turbidites with an age of Thanetian (late Palaeocene) to Ypresian (early Eocene) (Löffler, 2013). Samples A through F were collected but only A, B, D, and F used as these exhibited suitable, normal grading typical of a turbidite bed (Figure 1d). Similarly, the Strubach Section is also located in the Rhenodanubian Flysch zone, although approx. 23 km north of Salzburg in north-central Austria (location SF-1-6). Here the Altlengbach Formation, aged from late Maastrichtian (late Cretaceous) to Danian (early Palaeocene), comprises thin- to medium-bedded turbidites with clayey marlstones in the

upper sections (Figure 1e) (Egger, 2011). Two samples were collected here: A and B. The third sampling site at the Gamsbach creek in east-central Austria (location SF-1-8) is within the Gosau Group sandstones, part of the Zwieselalm Formation dated from the Palaeocene to the early Eocene (Egger et al., 2004; Koukal et al., 2022). Here, weakly cemented, thin turbidite beds with dark shales dominate and two samples: A, and B were collected (Figure 1f).

3.2. Sample Processing and Heavy-Mineral Separation

All samples were processed and analyzed at the Department of Sedimentology and Environmental Geology at Georg-August-University Göttingen. The turbidites were first broken manually with a hammer and then disintegrated using a disc mill, gradually decreasing the size until approx. 500 μm . The loose sediment for both the placers and the turbidites were dry sieved using a Retsch vibratory sieve shaker and split into <250, 250–500, and >500 μm grain-size fractions. The grain-size fractions less than 500 μm were treated with 5% acetic acid to digest any carbonates present, particularly important for the heavily carbonate-cemented samples. The samples were immersed and left until effervescence was no longer observed.

To further disaggregate the sediments and remove clay particles, each sample was placed in a wet sieving tower (Fritsch Analysette 3 Pro, 10 min run duration, amplitude 2.3 with a 5-s interval time). This split the sample into <63, 63–125, 125–250, and 250–500 μm grain-size fractions; the 30–63 μm size fraction was later separated using a smaller vibration wet sieve and 30 μm nylon mesh (for detailed information on this technique see Lünsdorf et al., 2023, this volume). All samples were washed, dried, and reduced (3–5 g per grain-size fraction) via the coning and quartering method to decrease user-initiated grain sorting (Hutton, 1950).

For heavy-mineral separation, each aliquot was placed into a 50 mL centrifuge vial, 40 mL of SPT (sodium polytungstate, density of 2.87 g/cm^3) solution added, shaken, and inserted into the centrifuge chamber. The Heraeus Multifuge X3R centrifuge ran at a rotation speed of 3,000 RPM over 10 min, for the finer fractions this procedure was completed twice to ensure complete separation. The bottom layer of the test tube containing the heavy-mineral fraction was frozen using liquid nitrogen and the remaining SPT liquid containing the light fraction was transferred into a set of filters. The frozen heavy-mineral fraction was defrosted and similarly extracted. All samples were washed several times with warm deionized water to remove any remaining SPT. Once the heavy-mineral fraction was dry, grains were embedded in epoxy resin (Araldite). Each resin mount contained only one grain-size fraction for all samples, thus separate mounts were created for each grain-size fraction (according to the Udden-Wentworth scale). Mounts were grinded and polished in multiple steps using SiC and Al_2O_3 abrasives to expose the grain interiors.

3.3. Heavy-Mineral Counting via Raman Spectroscopy

Conventionally, heavy-mineral analysis is performed by manually identifying and counting grains under a microscope using their optical properties. However, for this study, a large number of heavy-mineral grains is to be measured quantitatively, so small changes in compositions due to fractionation and sorting can be identified. Semi-automated Raman spectroscopy is a potentially non-destructive and relatively quick technique for identifying heavy minerals and can differentiate almost all mineral phases including polymorphs and opaque minerals based on their unique Raman spectra. This technique is well known and used as an effective tool for heavy-mineral studies (Andò & Garzanti, 2014; Andò et al., 2009; Chaudhuri et al., 2023; Dunkl et al., 2020; Lünsdorf et al., 2019; Schönig et al., 2023).

Before measuring, each mount was imaged using a Zeiss Axiolmager M2 microscope with a 20 \times objective, then using both transmitted and reflected light images, the measurement points for each grain were selected. To reduce selection bias, all mounted grains of each sample were measured according to Fleet (1926). Lists of measurement points were transferred to a Horiba XploRA Plus Raman microscope. Measurements were performed using a 532 nm laser, a 1,200 lines/mm grating covering a spectral range of 100–2,800 cm^{-1} with a spectral resolution of approx. 3.1 cm^{-1} , a 50 \times long-working-distance objective (NA 0.50), an automated exposure time estimated to reach 5,000 counts for each individual grain analysis (max. exposure time 20 s), and a reduced laser power based on the transmitted light gray value of each individual grain. Every 100 analysis were bracketed by an acetaminophen standard to correct for temporal drift. Lünsdorf et al. (2019) describes the setup, collection, and evaluation of Raman spectra in more detail.

3.4. Grain-Size Determination

For the loose beach placer deposits a Beckman Coulter LS13 320 laser particle size analyzer (LPS) was used. Thin sections were made for all turbidite samples and the longest visible axis of at least 200 random quartz grains were manually measured using a Zeiss Axioplan 2 microscope. As quartz is the major component of all turbidite samples, measuring 200 quartz grains per sample produces a good estimation for the overall grain-size distribution of a sample. Naturally, as the grains are presented in 2D in thin section, a correction equation from Harrell and Eriksson (1979) was used to estimate dimensions in 3D. This procedure is preferred over measuring the grain size of disintegrated turbidites by LPS as partial disintegration would cause a bias toward coarser grain-size.

3.5. Techniques for Identifying Grain-Size Inheritance

In order to distinguish heavy-mineral distributions as the product of hydrodynamics or grain-size inheritance, we need to first determine what a purely hydrodynamic-affected composition may look like. Resentini et al. (2013) applied the Stokes' and Impact laws, as mentioned in Section 2, to model sediment settling, size shifts, and thus, mineral distribution in various grain-size fractions. The Excel macro, named MinSORTING, takes mean sediment diameter, sorting, depositional medium (seawater, freshwater, or air), and sediment composition (chosen from nine varying tectonic settings) as its inputs. As its output, it gives the percentage contribution for 27 detrital sediment components for grain-size fractions of either 0.25, 0.5, or 1 phi. The model does not discriminate for phi >4, instead giving <63 μm . However, given the overall grain-size distribution of our turbidite samples within the sand range, the main mass of the heavy minerals within the <63 μm fraction can be assumed as falling within the 30–63 μm range (i.e., phi 4–5). The MinSORTING model gives the percentage proportion of a particular mineral in a grain-size fraction (e.g., 60% of all rutile have a grain size from 63 to 125 μm). The actual mineral counts were adjusted to the model by normalizing the mineral ratios from the model with those of the individual samples. This allows for comparison with the intermediate grain-size fraction (125–250 μm for the placers and 63–125 μm for the turbidites), to visualize the potential inheritance effects for the finer and coarser fractions. Small deviations from the model (i.e., 0.8 to 2 times the model output), are still considered as within hydraulic equivalence. Empty bars in the plots represent mineral pairings with combined grain counts below 100; this data is carefully considered and normally paired with other similar mineral pairings with higher counts before drawing conclusions.

Morton indices, proposed by Morton and Hallsworth (1994), use the relative abundances of two heavy minerals that should act similar through hydrodynamics. In comparison, these two mineral species should behave the same, independent of the grain-size fraction considered, if no other outside factors were at play. Therefore, intrasample variation of Morton indices should indicate factors other than hydrodynamics have had an impact on heavy-mineral compositions. For a statistically robust index, combined grain count of 100 is required for all Morton mineral pairings.

Principal component analysis (PCA) helps to analyze multi-dimensional data sets, here a biplot is used to visualize and help understand which minerals are producing the greatest variance within grain-size fractions and samples. The PCA biplot was produced using R (R Core Team, 2021) in RStudio (RStudio Team, 2022) using the built-in R function `prcomp`. Ternary diagrams are used here to compare the varying abundances of three minerals simultaneously, plots were produced using the TRI-PLOT Excel spreadsheet from Graham and Midgley (2000).

4. Results

4.1. Modern Beach Deposits

4.1.1. Grain-Size Distribution

All three beach samples have a distinct grain-size distribution, observable in the cumulative grain-size curves in Figure 2a. Sample EY-62-02, the darkest-colored placer deposit, contains the finest grain-size distribution with a median of 225 μm . The intermediate layer, EY-62-03, has a slightly coarser median grain size of 270 μm , and the “normal” beach sand (EY-62-01) is the coarsest of the three samples with a median of 367 μm . Between the coarsest and finest samples, there is a 0.61 phi difference in mean grain size. All samples are “moderately well sorted,” categorized by Folk and Ward (1957). These sorting values are important when calculating the “ideal” heavy-mineral distribution from Resentini et al. (2013). Based on the measured grain-size distribution, the three fractions 63–125, 125–250, and 250–500 μm were selected for further analysis.

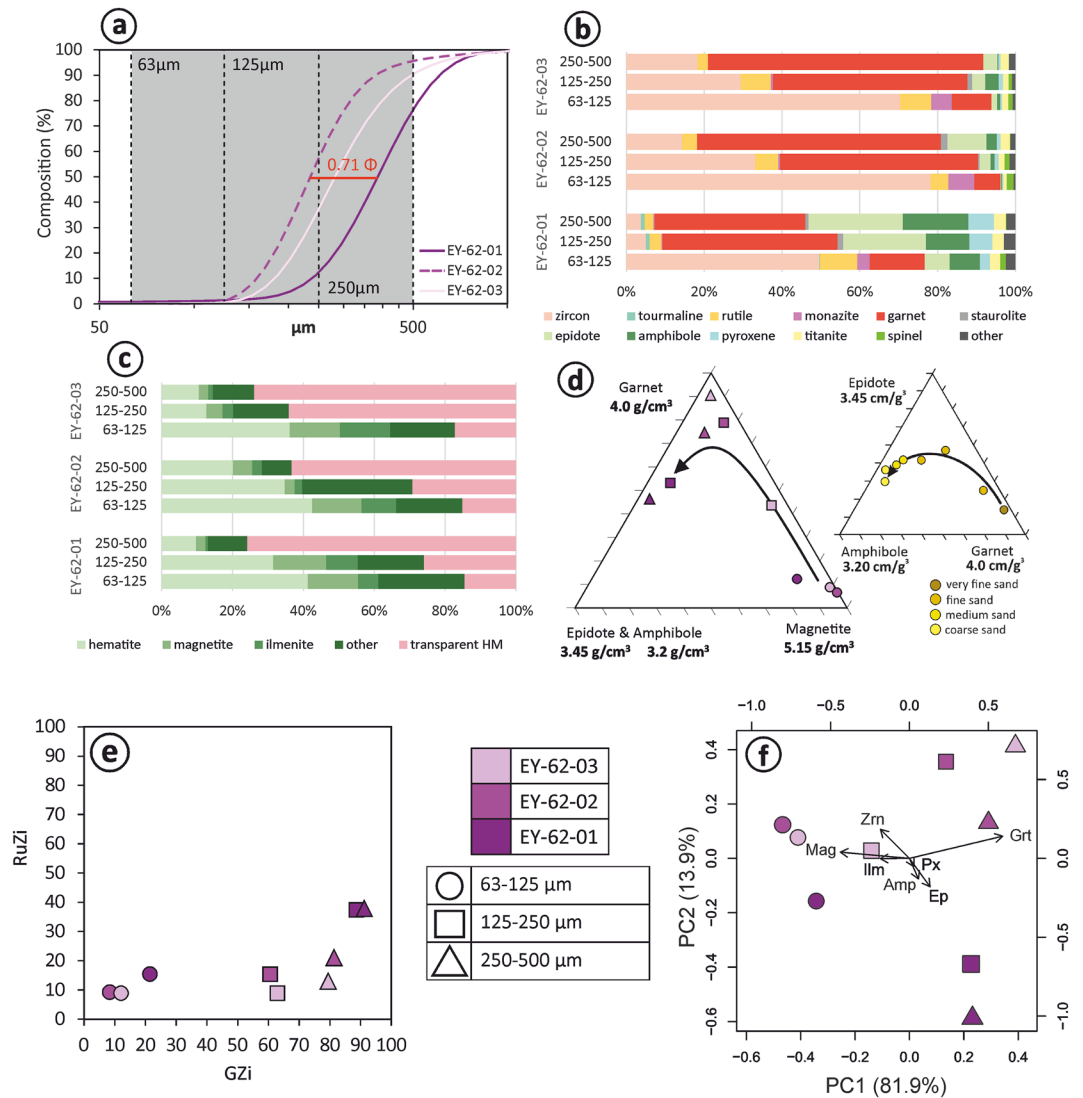


Figure 2. (a) Grain-size distribution plot for the three modern beach samples, with all analyzed grain-size intervals shaded in gray and median phi difference between samples shown in red. (b) Transparent heavy-mineral distribution for modern deposits, with percentage proportions along the X-axis, and samples and grain-size fractions on the Y-axis. (c) Opaque heavy-mineral distribution for each sample and grain-size interval. (d) Left: ternary plot with garnet, magnetite, and epidote and amphibole, with the arrow showing increasing grain size; right: ternary plot with garnet, amphibole, and epidote adapted from Garzanti et al. (2008). (e) Morton indices: garnet-zircon (GZi) versus rutile-zircon (RuZi) cross plot. (f) Principal component analysis biplot, with PC1 versus PC2.

4.1.2. Heavy-Mineral Composition

Heavy-mineral concentration (HMC) is highest for all samples within the 63–125 μm grain-size fraction (96%–100%). Samples EY-62-02 and -03 continue with considerably high HMC for both 125–250 μm (97%–99%) and 250–500 μm fractions (71%–84%), whereas for the background sediments of -01 HMC are only 13% and 1%, respectively. In terms of heavy-mineral composition, grain-size fractions of all samples have a transparent heavy-mineral suite dominated by garnet and zircon. All individual heavy-mineral percentage proportions and HMCs are given in Table 2; bar plots displaying transparent heavy-mineral compositions are shown in Figure 2b.

In the finest size fraction for all samples, 63–125 μm, zircon is the dominating transparent heavy mineral ranging from 50% to 78%, with the highest proportion being in the dark placer sample 02. Garnet, rutile, and monazite have the next largest proportions, although none contributes more than 15% of the overall transparent heavy-mineral assemblage. The background sand sample (01) also contains a considerable amount of amphibole

Table 2
Grain Percentages for Each Heavy-Mineral Species for All Modern and Ancient Deposits

| Sample | GS (μm) | HMC | Zrn | Tur | Rt | TiO ₂ | Ap | Mnz | Grt | Als | St | Ep | Amp | Px | Ttn | Spl | Sum |
|----------|---------|--------|------|------|------|------------------|------|-----|------|-----|------|------|------|-----|-----|-----|-------|
| EY-62-01 | 63–125 | 96.15 | 49.6 | 0.1 | 9.6 | 1.9 | 0.1 | 3.2 | 14.2 | 0.4 | 0.0 | 6.4 | 7.8 | 2.5 | 2.7 | 1.5 | 748 |
| | 125–250 | 12.66 | 5.1 | 1.0 | 3.0 | 0.9 | 0.1 | 0.2 | 45.4 | 1.1 | 1.5 | 21.5 | 11.2 | 6.0 | 3.0 | 0.0 | 820 |
| | 250–500 | 1.32 | 3.7 | 1.0 | 2.3 | 1.5 | 0.2 | 0.3 | 38.7 | 0.7 | 0.8 | 24.2 | 16.9 | 6.5 | 3.1 | 0.2 | 615 |
| EY-62-02 | 63–125 | 100.00 | 78.2 | 0.0 | 4.6 | 0.4 | 0.0 | 6.6 | 6.8 | 0.0 | 0.0 | 0.1 | 0.3 | 0.3 | 0.9 | 1.8 | 738 |
| | 125–250 | 98.94 | 33.1 | 0.0 | 6.0 | 1.1 | 0.0 | 0.4 | 50.9 | 0.4 | 0.4 | 2.8 | 1.1 | 1.1 | 1.5 | 1.3 | 468 |
| | 250–500 | 83.73 | 14.4 | 0.0 | 3.8 | 1.2 | 0.0 | 0.0 | 62.7 | 0.0 | 1.7 | 10.0 | 2.6 | 1.0 | 2.4 | 0.2 | 418 |
| EY-62-03 | 63–125 | 99.71 | 70.3 | 0.0 | 8.1 | 0.3 | 0.0 | 5.3 | 10.2 | 0.3 | 0.0 | 1.5 | 0.8 | 0.5 | 1.6 | 1.1 | 620 |
| | 125–250 | 97.26 | 29.4 | 0.0 | 7.7 | 0.9 | 0.0 | 0.6 | 50.0 | 0.0 | 1.1 | 3.4 | 3.4 | 1.1 | 1.4 | 0.9 | 350 |
| | 250–500 | 70.88 | 18.3 | 0.0 | 2.7 | 1.1 | 0.3 | 0.0 | 70.8 | 0.3 | 0.0 | 3.6 | 0.3 | 0.5 | 2.2 | 0.0 | 366 |
| SF-1-2A | 30–63 | 1.00 | 45.4 | 25.9 | 19.9 | ^a | 0.3 | 5.3 | 2.0 | 0.0 | 0.3 | <0.1 | <0.1 | 0.0 | 0.0 | 0.8 | 2,879 |
| | 63–125 | 0.34 | 13.6 | 30.4 | 51.8 | ^a | 0.0 | 2.1 | 0.2 | 0.0 | 0.0 | 0.0 | 1.2 | 0.0 | 0.0 | 0.7 | 427 |
| | 125–250 | 0.17 | 6.5 | 26.0 | 55.6 | ^a | 1.2 | 2.4 | 0.6 | 0.0 | 0.0 | 0.0 | 6.5 | 0.0 | 0.0 | 1.2 | 169 |
| SF-1-2B | 30–63 | 1.01 | 42.0 | 27.1 | 22.4 | ^a | 0.4 | 4.9 | 1.9 | 0.0 | 0.1 | 0.0 | <0.1 | 0.0 | 0.0 | 1.1 | 3,214 |
| | 63–125 | 0.36 | 12.3 | 36.0 | 47.9 | ^a | 0.8 | 2.6 | 0.0 | 0.0 | 0.0 | 0.0 | 0.4 | 0.0 | 0.0 | 0.0 | 495 |
| | 125–250 | 0.12 | 8.1 | 35.8 | 51.8 | ^a | 1.0 | 2.0 | 0.0 | 0.0 | 0.0 | 0.3 | 0.3 | 0.0 | 0.3 | 0.5 | 394 |
| SF-1-2D | 30–63 | 1.01 | 43.6 | 20.1 | 30.0 | ^a | 0.8 | 3.2 | 1.5 | 0.0 | 0.1 | <0.1 | 0.0 | 0.0 | 0.0 | 0.5 | 1,634 |
| | 63–125 | 0.46 | 6.6 | 26.3 | 58.2 | ^a | 0.3 | 1.3 | 1.1 | 0.0 | 0.0 | 0.0 | 4.7 | 0.0 | 0.0 | 1.6 | 380 |
| | 125–250 | 0.59 | 9.4 | 29.4 | 57.1 | ^a | 0.0 | 2.5 | 0.3 | 0.0 | 0.0 | 0.3 | 0.8 | 0.0 | 0.0 | 0.3 | 394 |
| SF-1-2F | 30–63 | 1.68 | 47.3 | 22.6 | 20.4 | ^a | 0.4 | 6.2 | 1.9 | 0.0 | 0.0 | 0.0 | <0.1 | 0.0 | 0.0 | 1.1 | 1,560 |
| | 63–125 | 1.42 | 13.9 | 34.7 | 46.8 | ^a | 0.9 | 2.3 | 0.5 | 0.0 | 0.9 | 0.0 | 0.0 | 0.0 | 0.0 | 0.0 | 216 |
| | 125–250 | 2.94 | 13.6 | 36.4 | 40.9 | ^a | 0.0 | 0.0 | 0.0 | 0.0 | 0.0 | 0.0 | 0.0 | 0.0 | 4.5 | 4.5 | 22 |
| SF-1-6A | 30–63 | 2.90 | 36.9 | 8.6 | 21.7 | ^a | 19.2 | 2.3 | 8.8 | 0.0 | 0.6 | 0.0 | 0.0 | 0.0 | 1.7 | 0.1 | 816 |
| | 63–125 | 2.22 | 11.8 | 21.0 | 22.2 | ^a | 28.3 | 2.0 | 9.0 | 0.0 | 1.6 | 0.0 | 2.0 | 0.0 | 1.1 | 0.9 | 442 |
| | 125–250 | 1.78 | 12.7 | 9.5 | 28.6 | ^a | 28.6 | 0.0 | 11.1 | 1.6 | 1.6 | 1.6 | 1.6 | 0.0 | 1.6 | 1.6 | 63 |
| SF-1-6B | 30–63 | 3.00 | 30.8 | 18.0 | 35.4 | ^a | 8.0 | 1.1 | 4.8 | 0.0 | 0.3 | 0.2 | 0.3 | 0.0 | 0.8 | 0.2 | 610 |
| | 63–125 | 1.97 | 19.4 | 22.0 | 38.8 | ^a | 10.4 | 1.1 | 4.5 | 0.0 | 0.4 | 0.7 | 0.4 | 0.0 | 0.0 | 2.2 | 268 |
| | 125–250 | 1.02 | 9.3 | 16.7 | 61.1 | ^a | 7.4 | 1.9 | 1.9 | 0.0 | 1.9 | 0.0 | 0.0 | 0.0 | 0.0 | 0.0 | 54 |
| SF-1-8A | 30–63 | 5.12 | 3.6 | 8.2 | 13.9 | ^a | 14.3 | 0.1 | 20.8 | 0.5 | 6.8 | 20.9 | 2.1 | 0.0 | 7.9 | 0.8 | 1,700 |
| | 63–125 | 3.39 | 1.0 | 10.6 | 25.2 | ^a | 7.3 | 0.4 | 27.7 | 0.3 | 9.3 | 5.4 | 6.5 | 0.0 | 6.1 | 0.3 | 710 |
| | 125–250 | 1.31 | 0.6 | 15.8 | 22.4 | ^a | 9.0 | 0.0 | 31.0 | 0.6 | 10.9 | 2.6 | 2.1 | 0.0 | 4.7 | 0.2 | 468 |
| SF-1-8B | 30–63 | 5.58 | 4.5 | 17.7 | 19.3 | ^a | 3.1 | 0.4 | 18.9 | 0.6 | 5.9 | 24.3 | 0.5 | 0.0 | 4.5 | 0.2 | 2,497 |
| | 63–125 | 2.45 | 1.2 | 17.7 | 30.2 | ^a | 3.8 | 0.1 | 21.0 | 0.7 | 8.3 | 8.1 | 5.4 | 0.0 | 3.1 | 0.4 | 851 |
| | 125–250 | 2.28 | 0.9 | 23.6 | 34.6 | ^a | 2.8 | 0.0 | 19.6 | 0.6 | 6.0 | 6.9 | 2.2 | 0.0 | 2.8 | 0.0 | 535 |

Note. HMC stands for total heavy mineral concentration and is given in weight percent. Total counts of transparent heavy minerals for each sample are in the final column. Mineral abbreviations follow Whitney and Evans (2010).

^aOther TiO₂ minerals (except from rutile) were not included for ancient deposits due to high likelihood of them not having a detrital origin. GS stands for grain-size interval.

(8%) and epidote (6%) which is not as prevalent in the other samples (<1.5%). The finest fraction contains the highest proportion of opaque minerals (hematite, magnetite, and ilmenite), contributing on average 84% of the total heavy-mineral assemblage (Figure 2c).

For the 125–250 μm fraction, the proportion of zircon decreases compared to the 63–125 μm fraction, and is generally replaced with a large increase in garnet. For samples 02 and 03, the proportion of garnet increases significantly from 7% to 51% and 10% to 50% of the whole composition, respectively. Alongside this, contributions of

minor minerals such as amphibole, pyroxene, and titanite also show small increases. Although decreased, zircon still contributes around 30% of the entire transparent heavy-mineral spectrum for both these samples. Sample 01 again displays more variation; amphibole and epidote are more frequent with proportions of 11% and 22% respectively, zircon proportion decreases dramatically from 50% to 5%, and garnet increases from 14% to 45%.

When comparing the intermediate (125–250 μm) and coarsest (250–500 μm) grain-size fractions for 01, the composition stays roughly similar, with some changes for garnet (45%–39%), amphibole (11%–17%), and epidote (22%–24%), and further small decreases of zircon and rutile. Looking at the coarsest fraction for 02 and 03, garnet is still increasing (63% and 71% of the total composition respectively), and zircon and rutile are decreasing. The distribution of opaque minerals, as mentioned earlier, continues the expected trend with only 24%–36% in the 250–500 μm fraction compared with much higher proportions in the finer fractions, hematite continues as the most prevalent opaque heavy mineral in all grain-size fractions (Figure 2c).

4.1.3. Further Heavy Mineral Evaluation

The heavy mineral results for all three modern beach samples and their three respective grain-size fractions were further analyzed using Morton indices and a compositional biplot based on PCA (Section 3.5).

High counts for garnet, zircon, and rutile allow for GZi (garnet-zircon) and RuZi (rutile-zircon) mineral pairings (Figure 2e). Grain-size fractions are widely separated along the GZi axis, with all samples within each fraction clustering together (except for the intermediate and coarsest fraction of EY-62-01). The finest grain size (63–125 μm) contains the lowest GZi ratio, with the relative abundance of garnet strongly increasing with grain size. The RuZi axis has considerably less variation with grouping within samples rather than grain-size fractions; samples trend from EY-62-03 to -02 to -01 with increasing RuZi, that is, the normal beach sand shows highest RuZi values.

When plotting magnetite (5.15 g/cm^3), garnet (4.0 g/cm^3), and epidote + amphibole (average of 3.33 g/cm^3) on a ternary plot, a clear trend of decreasing mineral density with increasing grain size can be recognised (Figure 2d, left). Garzanti et al. (2008) previously applied a similar plot to aeolian dunes originating from the Po Delta, proportions of epidote (3.45 g/cm^3), garnet (4.0 g/cm^3), and amphibole (3.2 g/cm^3) were compared for seven different grain sizes from 75 to 300 μm (Figure 2d, right). The very fine sand plots with the highest garnet composition, as grain size increases so does the epidote composition, with the coarsest sand shown to contain the highest proportion of amphibole, the least dense mineral. This same pattern is reflected in the placer deposits: all of the finest fractions plot in the high magnetite composition region, the intermediate fractions then transition toward the garnet region, with sample 02 having a considerably higher garnet component than 01 and 03. Finally, for samples 01 and 02 in the 250–500 μm fraction, relative proportions of (epidote + amphibole) increase. The heavy-mineral variation seen in each grain-size fraction is further demonstrated by a compositional biplot (Figure 2f). The first principal component (PC1), which describes most of the total variance within the samples and grain-size fractions (82%), highlights the large contrast between magnetite and garnet, with fine grain sizes on the magnetite side of the plot and vice versa. The second principal component, accounting for 14% of the total variance (PC2), splits zircon with (amphibole + epidote), showing the latter are more significant within sample EY-62-01, compared to samples -02 and -03.

4.2. Ancient Turbidite Deposits

4.2.1. Grain-Size Distribution

As expected, when sampling turbidite successions, samples at each location show normal grading with the base sample containing the coarsest grain size, and it subsequently decreasing up through the individual turbidite beds (Figure 3a). The four samples originating from the quarry in Höflein have a variation in median grain size of 0.54 phi between the coarse base and fine uppermost sample. In all samples, approx. 84%–97% fall between the 63–250 μm size fraction and all are classified as “well sorted” (Folk & Ward, 1957). The Strubach section has a higher difference of 0.95 phi between the two samples, with the median grain diameter of sample A and B, 128 and 66 μm respectively; these samples are categorized as “moderately well sorted.” The greatest variation in median grain size is found in the Gamsbach samples with a difference of 1.55 phi, here the coarser sample A (median grain size of 278 μm) is not as well sorted as the B sample (median grain size of 95 μm). Based on the

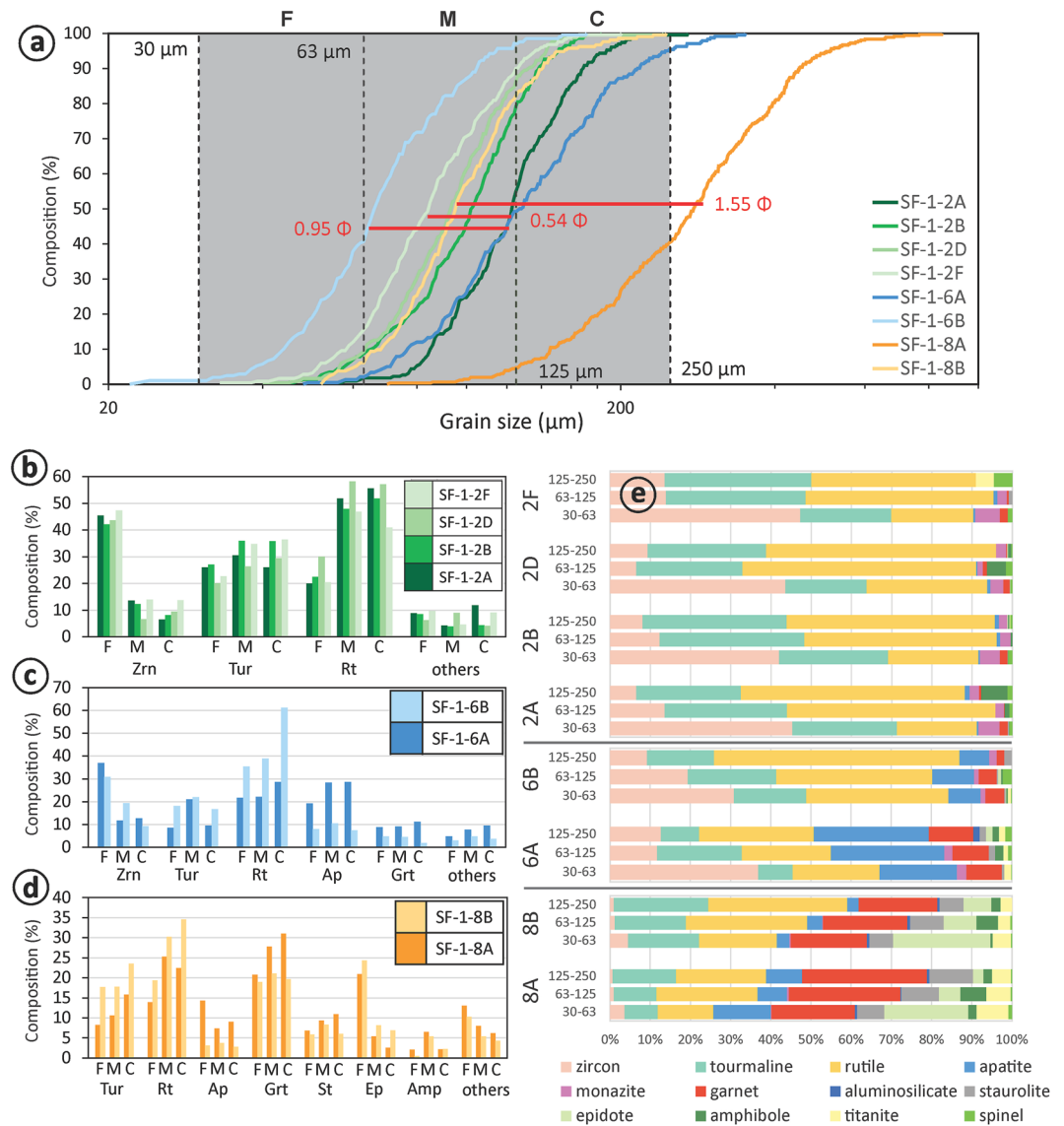


Figure 3. (a) Grain-size distribution plots for ancient turbidite deposits, with the shaded area representing the chosen analyzed grain size fractions (63–125, 125–250, and 250–500 μm), and the red lines showing the phi difference between each location's median. (b) Heavy mineral assemblage for Höflein quarry with prevalent minerals, at each mineral, grain-size fraction increases from left to right with fine ($F = 30\text{--}63 \mu\text{m}$), medium ($M = 63\text{--}125 \mu\text{m}$), and coarse ($C = 125\text{--}250 \mu\text{m}$). (c) Heavy mineral assemblage for Strubach section with prevalent minerals. (d) Heavy mineral assemblage for Gamsbach with prevalent minerals. (e) Transparent heavy-mineral assemblages for each sample and grain-size fraction (Y -axis), and their percentage proportions (X -axis), with a colored key for all minerals at the bottom.

measured grain-size distribution, the three fractions 30–63, 63–125, and 125–250 μm were selected for further analysis for all turbidite samples.

4.2.2. Heavy-Mineral Composition

Heavy-mineral percentage distributions and HMCs are contained within Table 2; intersample comparisons between the most prevalent minerals for each location is in Figures 3b–3d; bar plots displaying transparent heavy-mineral compositions are contained within Figure 3e. For all turbidite samples, TiO_2 mineral proportions (i.e., brookite, anatase, and other intergrowths) have not been included, this was decided after further optical analysis, which suggested a high likelihood of them being authigenic rather than detrital. HMC is highest in the 30–63 μm grain-size fraction ranging between 1.0% and 5.6%, and lowest within the 125–250 μm fraction (0.1%–2.9%). On first observations, it is clear that variability among grain-size fractions is far greater than

between samples for the highly stable ZTR-dominated (zircon, tourmaline, and rutile) Höflein quarry samples (location SF-1-2; Figures 3b and 3e). This is especially noticeable for the 30–63 μm fraction, compared to the coarser 63–125 and 125–250 μm fractions. Zircon is highest in the 30–63 μm fraction, at around 45%, and decreases to 7%–14% in the two coarser grain-size fractions. This large decrease in zircon is mostly countered with a considerable increase in rutile, in addition to a minor increase in tourmaline. Proportions of both these minerals stay relatively constant in the 63–125 and 125–250 μm grain-size fraction. Minor minerals: monazite, garnet, spinel, amphibole, and apatite together do not contribute more than 12% of the total assemblage in any grain-size fraction, although proportions of monazite and garnet are highest in the 30–63 μm fraction.

The two samples from the Strubach turbidite contain a ZTR- plus apatite-dominated assemblage (location SF-1-6; Figures 3c and 3e). For sample A, proportions of ZTR are averaging 58% over all grain sizes, while in B this proportion stands considerably more at 84%. To make up for this difference in A, apatite, garnet, and other minor minerals (e.g., monazite and staurolite) all contribute more. Furthermore, these minerals are most common in the coarsest fraction with apatite increasing from 19% to 29% between 30–63 and 125–250 μm , and garnet from 9% to 11%. Within the high ZTR composition of sample B, zircon is decreasing with increasing grain size and being replaced with rutile. Meanwhile, tourmaline proportions stay relatively constant with small increases in the intermediate fraction (63–125 μm).

The Gamsbach heavy-mineral assemblages are most diverse with varying high proportions of tourmaline, rutile, apatite, garnet, staurolite, epidote, and titanite (location SF-1-8; Figures 3d and 3e). Unlike other locations, ZTR for both samples increases noticeably from 30–63 to 125–250 μm , mostly a result of large increases in rutile. Garnet proportions are highest and have the most variation in the base sample A, ranging from 21% to 31% from the finest to coarsest fractions, compared to 19%–21% for B. Staurolite slightly increases with grain size for sample A, peaking at 11%, but is more stable for sample B, peaking at 8%. Decreasing trends from finest to coarsest grain size in both samples are present with epidote, titanite, and apatite. Amphibole peaks at around 5%–7% in the intermediate fraction of both samples.

4.2.3. Further Heavy Mineral Evaluation

For the Höflein section, TZi (tourmaline-zircon) and RuZi (rutile-zircon) mineral pairings were selected for comparison (Figure 4a). Both mineral pairings clearly separate the finest grain-size fraction (30–63 μm) from the two coarser fractions (63–125 and 125–250 μm), with almost no distinction between individual samples. Both TZi and RuZi increase with increasing grain size, meaning higher proportions of zircon within the fine fractions is detected, relative to tourmaline and rutile, respectively. Similar patterns are seen within the ternary plot, which compares the relative abundances of zircon (4.65 g/cm³), rutile (4.25 g/cm³), and tourmaline (3.15 g/cm³) for each grain size and sample (Figure 4b). The trend of increasing lower density minerals with increasing grain size is observable between zircon and rutile, but is not apparent for rutile versus tourmaline. In Figure 4c PC1 describes approx. 93% of the total variance, widely separating zircon and rutile. The finest grain-size fraction for all samples clusters close to the zircon pole whereas all coarser grain-size fractions plot on the rutile side. PC2 only describes approx. 5% of the total variance, mostly related to tourmaline. Yet, there is little pattern visible between grain size and samples along PC2.

Due to the different mineral abundances present in the Strubach section, the following mineral pairings were selected for comparison: ATi (apatite-tourmaline) against ZTi (zircon-tourmaline) and GRui (garnet-rutile) against ZRui (zircon-rutile). The two samples SF-1-6A and SF-1-6B clearly separate along the ATi axis, with variation between grain-size fractions less important (Figure 5a). This is the opposite for ZTi, where the 30–63 μm fraction for both samples plot with the highest values, and the other two fractions show no particular relation to grain size. Although, it is worth noting that three out of the four coarser fractions (63–125, 125–250 μm) do not reach the minimum grain count of 100. A similar pattern is displayed for the GRui versus ZRui plot, with GRui separating samples and ZRui separating grain-size fractions (Figure 5b). Notably, ZRui values clearly increase with decreasing grain size (i.e., there is more zircon relative to rutile in the finer grained grain size fractions). The observed separation between samples is further exemplified in the biplot. The PC1, representing ~63% of the sample variance, mostly splits apatite and rutile, while the PC2, describing ~30% of the total variability, splits zircon and apatite (Figure 5c). All grain sizes for SF-1-6A plot in the left half of the plot, with major influences from zircon (for the 30–63 μm fraction), and garnet + apatite (for the 63–125 and 125–250 μm fractions). Conversely, all the SF-1-6B fractions plot on the right side with significant minerals zircon (mostly for the 30–63 μm fraction) and rutile (mostly for the 125–250 μm fraction).

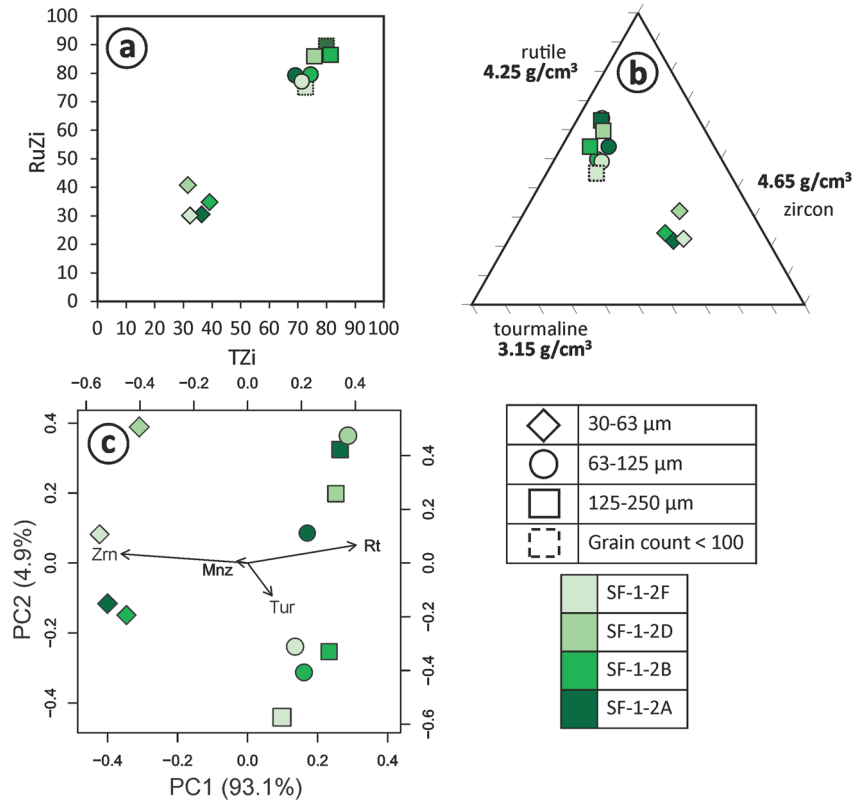


Figure 4. Analysis of heavy-mineral content for the Rhenodanubian flysch sandstone sample of the Höflein quarry. (a) Tourmaline-zircon (TZi) versus rutile-zircon (RuZi) cross plot (symbols outlined in a dotted line relate to those samples with mineral pair counts below 100). (b) Ternary diagram showing the relationship between zircon, rutile, and tourmaline with increasing grain size and density. (c) Principal component analysis including those minerals with highest abundance: zircon, rutile, tourmaline and monazite.

Likewise, two samples with three grain-size fractions were collected and analyzed for the Gamsbach location. The indices chosen for these samples were GRui (garnet-rutile), ATi (apatite-tourmaline) and GTi (garnet-tourmaline). First, the ATi axis (used for both plots) again separates the two samples nicely, with SF-1-8A altogether having higher proportions of apatite compared to SF-1-8B (Figures 5d and 5e). This is identical to the Strubach section samples, where the base sample SF-1-6A also contains the highest abundance of apatite relative to tourmaline (Figure 5a). Furthermore, both the GRui and especially GTi axes for the two plots separate SF-1-8A and SF-1-8B, but they are considerably less distinct than ATi (Figures 5d and 5e). Apart from the separation of the A and B samples (which within itself presents a significant grain size contrast; Figure 3a), the individual grain-size fractions do not follow a clear trend. As this sample set contains a largely diverse heavy-mineral spectrum, more minerals are represented on the PCA biplot. PC1 describes approx. 60% of the total variability and mostly splits epidote and rutile, and PC2 shows approx. 32% of the variance, mostly splitting garnet and apatite versus tourmaline (Figure 5f). The biplot separates the samples clearly with SF-1-8B segregated in the bottom half, with most influence from rutile, tourmaline, and epidote. SF-1-8A grain-size fractions all plot in the top half, with garnet, apatite, and staurolite the most influential. It is also interesting to observe the clear grain-size pattern presented, with the 30–63 μm fraction strongly affected by epidote whereas the two coarser fractions split off with SF-1-8A tending toward garnet at the top of the plot and SF-1-8B toward tourmaline and rutile at the bottom of the plot.

5. Discussion

5.1. Modern, Placer-Bearing Beach Sand Deposit From Denmark

The modern Denmark beach samples present an excellent analogy for sediment that should typically produce well hydrodynamically sorted deposits, except modification from re-entrainment (see Section 2.1). The three

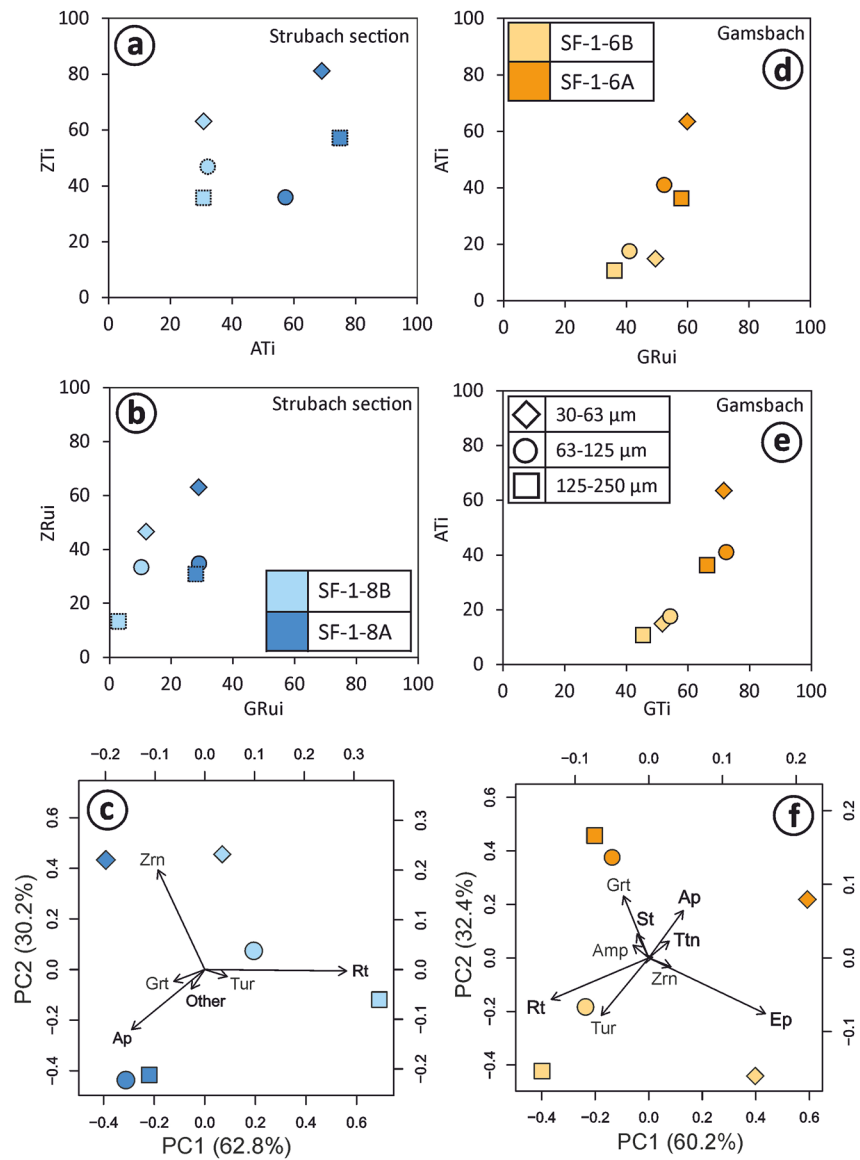


Figure 5. Analysis of heavy-mineral content for the ancient deposits Strubach section and Gamsbach. Symbols with a dotted outline within the cross plots relate to samples with mineral pair counts below 100; the “other” category within the Principal component analysis (PCA) biplots represent all other minerals present which only have minor significance to the sample variance; the darker color for each sample set represents the base layer. (a) Apatite-tourmaline (ATi) versus zircon-tourmaline (ZTi) cross plot for the Strubach section. (b) Garnet-rutile (GRui) versus zircon-rutile (ZRui) cross plot for the Strubach section, (c) PCA biplot for the Strubach section with PC1 plotted against PC2. (d) Garnet-rutile (GRui) versus apatite-tourmaline (ATi) cross plot for Gamsbach. (e) Garnet-tourmaline (GTi) versus apatite-tourmaline (ATi) cross plot for Gamsbach. (f) PCA biplot for Gamsbach with PC1 against PC2.

individual layers contain distinct grain-size distributions and heavy-mineral assemblages, in addition to strong mineral variations between grain-size fractions within each layer. There is a 0.71 phi difference between the finest and coarsest layer, with the finest layer being the darkest placer deposit, reflecting the most pronounced HMC. On first observations regarding the transparent heavy minerals, in all samples zircon concentrates in the finer fractions and garnet in the coarser fractions. Considering the principle of hydraulic equivalence, this relationship is expected, with garnet ($\sim 4.0 \text{ g/cm}^3$) having a lower density than zircon ($\sim 4.65 \text{ g/cm}^3$). This is mirrored by abundances of dense opaque minerals reaching 85% within the finest fraction (63–125 μm , Figure 2c), that is, hematite (5.04 g/cm^3), magnetite (5.15 g/cm^3), and ilmenite (4.72 g/cm^3). However, further insight into the proportions of these particular minerals within each grain-size fraction is important to understand whether the effects are a pure result of hydrodynamics, or, whether grain-size inheritance also plays a role.

5.1.1. Are Hydrodynamic Effects the Main Controlling Factor?

If hydrodynamic processes were the main controlling factor on the abundance of heavy minerals within these sediments during transport and deposition, those minerals with similar densities and shapes are expected to settle together (Garzanti et al., 2008; Rubey, 1933a). This hypothesis is tested by comparing the relative abundances via Morton indices (Figure 2e; Morton & Hallsworth, 1994). Variations within the mineral crossplots may suggest influence from factors other than hydrodynamics. Morton indices have previously been applied to understand changing provenance indicators within a succession (e.g., Hounslow & Morton, 2004; Morton & Hallsworth, 1994; Morton & Hurst, 1995). However, here they are applied to samples collected from modern beach sands, where sedimentary processes and hydrodynamics may change but the provenance signal is expected to stay constant.

The increasing GZi index (i.e., greater proportions of garnet) with increasing grain size is the expected when following hydrodynamic trends (Figure 2e). However, for the samples within each grain-size fraction, sample 01 outlies from the others, with 02 and 03 plotting relatively close together for all three grain-size fractions. Sample 01 (Figure 1b) is the background “normal” sand sample, which due to its lower concentration of heavy minerals, has likely not undergone the same processes during formation as the other two samples. Placer deposits have a greater rate of reworking, including re-entrainment sorting, allowing for the removal of coarser light minerals and the concentration of finer heavy minerals (Komar & Wang, 1984; Slingerland, 1977, 1984). This would produce an assemblage differing in proportions of garnet, zircon, and rutile; therefore, not aligning with the background sedimentation. Clear hydrodynamic trends are also found in Figure 2d within the ternary plot. The size-density trend displays a transition with increasing grain size from high to low mineral density: the finest interval (63–125 μm) is most enriched in magnetite (5.15 g/cm^3), with increasing grain size the abundance of garnet (4.0 g/cm^3) increases, followed by epidote and amphibole (3.45 and 3.2 g/cm^3 , respectively). This hydrodynamic trend is clearly followed for samples 01 and 02, but the increase in epidote and amphibole between the intermediate and coarsest fraction is not seen for sample 03. The biplot additionally portrays the enrichment of the densest heavy minerals (magnetite, ilmenite, and zircon) within the finest grain-size fraction (Figure 2f). The high variability along PC1 mainly splits garnet and magnetite, two minerals with contrasting densities. The finer grain-size intervals are noticeably clustered near magnetite, with the lighter garnet being more significant for the coarser grain-size fractions. Due to high numbers of opaque minerals within these samples, the proportions in comparison to transparent minerals was evaluated, finding the highest opaque minerals concentration within the finest fraction. Proportions of opaque minerals then decrease with increasing grain size. This trend is directly related to hydrodynamics as opaque minerals have high mineral densities, therefore allowing them to concentrate in the finer portions of the sediment.

5.1.2. Is Grain-Size Inheritance a Relevant Factor?

Until now, the data presented has shown that hydrodynamics are certainly a dominating factor during deposition for the modern beach deposits. Nevertheless, these methods are unable to quantify whether the heavy-mineral compositions observed directly follow what is expected during hydrodynamic sorting and placer formation. MinSORTING (see Section 3.5) produces an “ideal” percentage distribution, under purely hydrodynamic sorting, based on inputs measured directly from each sample (Resentini et al., 2013). By observing the ratio between the compositions produced by MinSORTING and acquired heavy-mineral data, deviations from the model can be identified (Figure 6a, red arrows). According to the “Sample composition” characteristics set by Resentini et al. (2013), which aid in estimating an accurate bulk grain density, all beach deposits have been assigned to the “Recycled Clastic” sample composition category.

Four heavy-mineral ratios have been chosen to aid in the comparison between data sets (Figure 6a). While contrasts for the Zrn/Rt ratio are rather limited, the Zrn/Grt ratio clearly displays a significant increase in proportion of zircon, or alternatively a lack of garnet in the 63–125 μm interval, with all three samples having the Zrn/Grt ratio 8–11 times greater than that predicted from MinSORTING. This factor is higher than any potential uncertainty related to a one-phi-grain-size window. Additionally, for the 250–500 μm fraction, samples 02 and 03 are lower than expected with ratios at 0.6 and 0.7, respectively. Similarly, the Rt/Grt ratio shows higher values than hydrodynamically expected for the finest grain-size fraction, but lower values for the coarsest fraction. In addition, for the Grt/(Ep + Amp) ratio, although mineral counts are low for the 63–125 μm interval, garnet is presenting with much lower proportions than the model with values at approximately 0.4 for all samples. In contrast, the 250–500 μm fraction shows increased proportions of garnet in sample 03 (see also Figure 2b). These results strongly call for an inherited lack of fine-grained garnet (i.e., predominance of coarser-grained garnet), compared to the grain-size distribution expected from purely hydrodynamic sorting. This effect has obviously

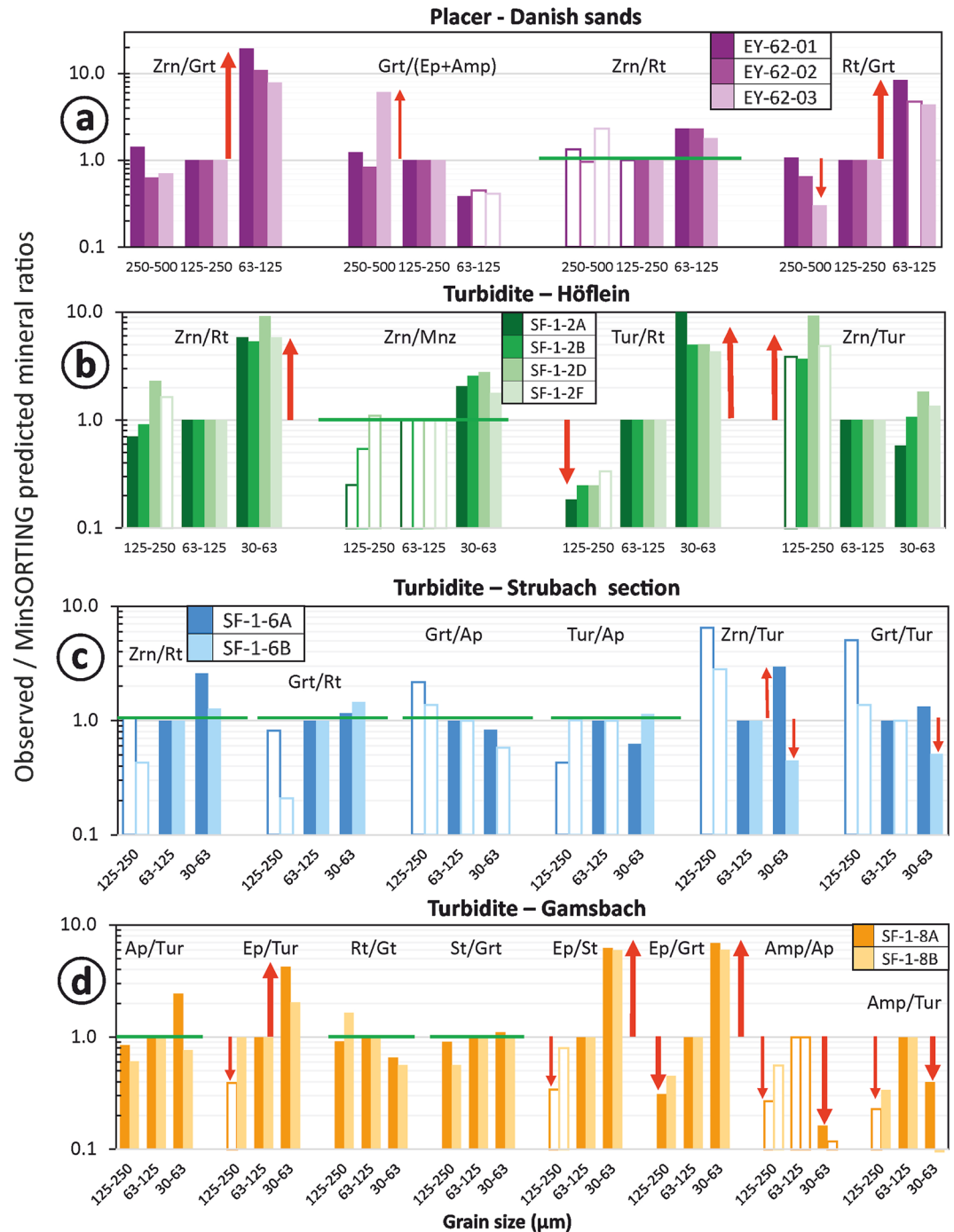


Figure 6. MinSORTING comparison plots for modern placer deposits (a), and turbidite layers (b). Unfilled bars relate to those mineral pairs with counts below 100 grains. Note that the medium grain size fraction has been normalized to one so that deviations from the model toward both fine and coarse are highlighted. Red arrows represent deviations from the model, green lines show mineral pairings where the model agrees with the measured heavy minerals.

survived long distance wind and glacial transport from Scandinavia and subsequent marine reworking and final deposition at a high-energy shoreline (Doody, 1991).

Interestingly, a similar trend is observed in the beach placer samples of Garzanti et al. (2008; their Figures 7 and 8D) where size shifts for zircon are higher and those for garnet are lower than the theoretical model, implying smaller zircon and larger garnet grain size than hydrodynamically expected.

5.2. Turbiditic, Graded Sandstone Beds of the Eastern Alps

The heavy-mineral spectra, measured here for three Paleogene turbidite locations, give an excellent insight into the changing mineral proportions both up section through individual turbidite beds (intersample) and between grain-size intervals within each sample (intrasample). All sample collections for each location vary in median grain size by 0.54–1.55 phi (Figure 3a). Theoretically, this grain-size variation exceeds most mineral size shifts (in comparison to quartz; Garzanti et al., 2008); meaning that heavy-mineral changes resulting from size-density sorting should be clearly observable. In addition, each location has a unique heavy-mineral assemblage (Figure 3c), meaning the proposed effect of grain-size inheritance can be explored for several mineral assemblages and various provenance signatures.

The Höflein sample set represents a durable residual heavy-mineral assemblage, with an abundance of ZTR minerals making up ~90% of all transparent heavy minerals counted. Thus, these sediments have a high compositional maturity, likely resulting from sediment recycling and/or undergoing processes that reduce proportions of less stable minerals (through chemical weathering, diagenesis etc.). Strubach samples are slightly more diverse, with higher proportions of apatite and garnet alongside high proportions of ZTR. The Gamsbach sample set presents the most varied heavy-mineral spectrum with minerals from both ZTR alongside less durable metamorphic minerals (e.g., garnet, staurolite, epidote, and titanite) and apatite, typically signifying a mix of provenance sources. However, the provenance of these sediments is beyond the scope of this study, instead it focusses on how the abundance of these minerals changes up-section within one sandstone bed, and how they may deviate from their expected “hydraulic equivalence” behavior.

5.2.1. Are Hydrodynamics Effects the Main Controlling Factor?

When comparing the heavy-mineral assemblages for all three turbidite locations, there are some stark contrasts to be found. The Höflein location has very little variation to be seen between samples within the single turbidite bed (Figure 3b). Moreover, significant differences between grain-size fractions are apparent, especially between the finest (30–63 μm) and two coarser (63–250 μm) fractions, which is the expected when taking size-density sorting into consideration. In contrast, both Strubach and Gamsbach locations have higher variation between the base (A) and top (B) samples, irrespective of grain-size fraction. The greatest deviation is observed between the coarser fractions (125–250 μm) of the Strubach samples where the proportion of rutile for SF-1-6B is more than double that of SF-1-6A (Figure 3b). Both Strubach and Gamsbach still show differences between grain-size fractions but intrasample variation is, for the most part, less than intersample variation (Figures 3c and 3d).

For the turbidite samples, there is heavy-mineral data that agrees with hydraulic processes; examples include strong decreases in proportions of zircon with increasing grain size for both Höflein and Strubach, and increases of garnet with increasing grain size for Gamsbach. However, several observations do not align with the effects from hydrodynamics. All locations show increases of rutile with increasing grain size (Figures 3b–3d). Rutile has a roughly similar density to zircon, meaning these minerals are expected to present similar trends with changing grain size. In addition, Figure 4a shows a similar grain-size pattern for both RuZi and TZi indices at Höflein, with a large divergence between 30–63 μm and the two coarser fractions. However, the density contrast between tourmaline and zircon is much greater than that for rutile and zircon, suggesting a lack of hydrodynamic control. Similarly, grain size follows the decrease in density from zircon to rutile, but the 125–250 μm grain-size interval does not deviate at all from the 63–125 μm cluster (i.e., there is no significant change for rutile vs. tourmaline, despite the large difference in density; Figure 4b). In the biplot, zircon and rutile are significantly separated by PC1 indicating their differing abundances are undoubtedly causing the greatest amount of variability within the samples (Figure 4c).

The deviation between A and B samples for both Strubach and Gamsbach is unexpected, yet intriguing. Both locations contain different provenance signatures, and each set is collected from a ~20–30 cm section within a single turbidite bed. This implies that changes in provenance from A to B should be ruled out as the cause of this effect. However, it is interesting to note in the biplot that the very same minerals are causal for the separation at each location (Figures 5c and 5f). For both base layers (SF-1-6A and SF-1-8A) apatite and garnet are significant, and for the top layers (SF-1-6B and SF-1-8B) rutile and tourmaline are important. Consequently, hydrodynamics can be also ruled out as the main reason for the contrast between A and B samples from both locations, as the hydrodynamically largely equivalent minerals apatite and tourmaline, have opposing behaviors (similarly, the much denser minerals garnet and rutile also show opposing behavior).

5.2.2. Is Grain-Size Inheritance a Relevant Factor?

The MinSORTING model has been applied to all turbidite samples in order to calculate “ideal” heavy-mineral proportions, considering mean grain size, sorting values, and depositional setting (Resentini et al., 2013). Sample composition for each location was selected as follows: “Recycled Clastic” for Höflein and Strubach, and “Subducted axial belt” for Gamsbach.

Four mineral ratios were selected to represent the Höflein samples (Figure 6b). Immediately noticeable is the large increase for Zrn/Rt ratio in the finest fraction (30–63 μm), with the observed ratio 5–9 times higher than the model prediction. The Tur/Rt ratio shows a similar pattern with large increases in the finest fraction from 4 to 10 times greater than the model. In addition to this, the coarsest fraction (125–250 μm) shows a major decrease (~ 0.2 – 0.3 compared to the model). The increases in the finest fraction for Zrn/Rt and Tur/Rt ratios suggest a potential lack of rutile, that is, coarser rutile grain sizes are preferentially delivered from the source rocks. Increases in the Zrn/Tur ratio within the coarsest fraction propose either an increasing proportion of coarse zircon or lack of coarse tourmaline within the samples. As Tur/Rt is also strongly decreased in the coarsest fraction, a lack of tourmaline in the coarsest fraction is most likely. The Höflein section thus reveals grain-size inheritance with respect to rutile (absence in the finest fraction) and tourmaline (absence in the coarsest fraction).

Six mineral ratios were chosen to represent the Strubach samples (Figure 6c). Four of them stay within 0.8–2 of the model (Zrn/Rt, Grt/Rt, Grt/Ap, and Tur/Ap ratios), meaning the effects of hydrodynamics roughly align with the observed heavy-mineral distribution. Particularly the minerals mainly responsible for the separation between A and B samples such as rutile, garnet, and apatite largely follow the hydrodynamic model (ratios Grt/Rt and Grt/Ap). However, larger deviations can be observed for Zrn/Tur and Grt/Tur, both being higher than hydrodynamically expected in the finest fraction of sample SF-1-6A but lower in SF-1-6B (e.g., Zrn/Tur varies from a factor of ~ 3.0 for 6A to ~ 0.4 for 6B). In addition, although results for the 125–250 μm fraction should be considered with caution due to the low number of counts, both these ratios are higher than expected, especially for SF-1-6A. These observations suggest a lack of coarse tourmaline as a possible feature inherited from the source.

Eight mineral ratios were selected for Gamsbach (Figure 6d). The minerals mainly in control of the separation between SF-1-8A and SF-1-8B such as rutile, tourmaline, garnet, and apatite largely follow the hydrodynamic model (ratios Ap/Tur and Rt/Grt)—with no evidence for potential grain-size inheritance. By contrast, Ep/Tur, Ep/St, and Ep/Grt all present the same trend: large increases for both samples (SF-1-8A and SF-1-8B) within the finest fraction (30–63 μm). This is also paired with some decreases for the coarsest fraction (125–250 μm) compared to the model, most significant for Ep/Grt. With epidote being the common nominator in these ratios, it can be proposed that there is an enrichment of epidote with the finer fractions for these samples, which is most likely a consequence of grain-size inheritance. Both Amp/Ap and Amp/Tur show considerable decreases in both the finest and coarsest fractions, resulting from a higher proportion of amphibole grains within the intermediate grain-size fraction (63–125 μm). Also visible in the bar plots of Figures 3d and 3e, this is likely a result of inherited grain sizes for amphibole and a lack of fine and coarse grains from the source.

5.3. Mechanical Effects

Both transportation of grains from source to sink and sample preparation methods exert mechanical stress and can lead to grain-size reduction. These mechanical effects, causing breakage, abrasion, and fragmentation need to be taken into account when considering the effects of grain-size inheritance. The mechanically most sensitive minerals, that is, those with a low relative mechanical stability and pronounced cleavage like pyroxene and amphibole, should be increased within the finer fractions relative to coarser fractions and more durable minerals. Previous experimental studies have attempted to deduce the relative stability of the most common heavy minerals (Dietz, 1973; Freise, 1931; Thiel, 1945). However, when this theory was applied to nature, no evidence was found to suggest that the heavy-mineral assemblage reduces in diversity over time (Morton, 2012). Examples from very long river systems such as the Nile (Garzanti et al., 2006), Brahmaputra (Garzanti et al., 2010), and Rhine (van Andel, 1950) all show no or very little noticeable change in heavy-mineral composition and associated provenance signatures. Similarly, no evidence of this is observed in the samples of this study. Using amphibole and pyroxene as examples, an enrichment in the finer fractions of both the beach sands and turbidite deposits is absent (Figures 2 and 3e).

The same principle idea of mechanical stability can be applied when considering the influence of laboratory methods utilized in this study. Those minerals with a lower mechanical stability and greater cleavage could be

further broken down during the milling of the hard rock samples, leaving them significantly smaller than their initial grain size. The epidote enrichment in the 30–63 μm fraction within Gamsbach samples could be linked to sample crushing but the enrichment of amphibole, a mineral with more pronounced cleavage than epidote, within the 63–125 μm fraction vetoes this (Figure 6d). Moreover, we have found several mineral pairings that have similar mechanical stabilities but contrasting proportions. For instance, a strong contrast between rutile and zircon proportions from coarse to fine for Höflein and Strubach turbidite samples (Figure 3e).

5.4. Influence From Imperfect Sampling

In an ideal world, a “perfect” clastic sediment sample, in terms of perfectly reflecting hydrodynamic equivalence, would consist of one single sedimentation layer. Practically this is a difficult, if not impossible feat, with these suggested layers often being mere millimeters thick. Therefore, samples are usually collected from macroscopically homogenous layers where effects of hydrodynamic disequivalence are thought to be minimized. This approach is practically inevitable when sampling clastic rocks and a sensible and pragmatic one when sampling loose sediment.

For the Denmark case sand samples were taken from several cm-thick units (see Figure 1b), likely comprising multiple sedimentation layers, allowing for the collection of sufficient material needed for analyses. Even though multiple sedimentation layers for each sample were likely collected, roughly similar grain size and color suggest roughly similar hydrodynamic conditions (under macroscopic conditions at the sampling site). Sample EY-62-03, which is most affected by mixing sedimentation layers of varying hydrodynamic conditions (see light colored lenses in Figure 1b), however, shows the very same evidence for grain-size inheritance, compared to the other samples. Zrn/Grt and Rt/Grt ratios present clear deviations from the hydrodynamic model for the very fine sand fraction regardless of sample, such that both “end-members”, in this case the placer and background “normal” beach sedimentation, show the same features. The deviations in mineral ratios may reach about an order of magnitude (Figure 6), and thus common variability due to sample preparation or occasional erroneous mineral classification are insufficient to explain these observations (Dunkl et al., 2020). The data simply reflect a lack of garnet in the 63–125 μm fraction. The main contrast of the “mixed sample”, EY-62-03, compared to the others is an increase in garnet over (epidote + amphibole) in the 250–500 μm fraction compared to the hydrodynamic model (Figures 2d and 6a). This may have been influenced by the mixing of layers during sampling but anyway the evidence for grain size inheritance still stands, that is, enrichment of garnet in the coarser fractions, in line with its decrease in the finer fractions.

5.5. Diagenetic Effects

Characterizing the considerable effect diagenesis can have on the heavy-mineral assemblage of ancient deposits is incredibly important (e.g., Garzanti et al., 2018; Morton & Hallsworth, 1999; Turner & Morton, 2007). The fact that drastic changes may occur in the abundances of certain heavy minerals due to chemical dissolution during burial is well known (e.g., Gazzi, 1965). By looking at the type and prevalence of particular heavy minerals, alongside the HMC, it should be apparent whether (or to which degree) the assemblage reflects its primary provenance signatures. For example, if there is a high HMC and an abundance of typically unstable minerals, then the likelihood of a primary composition with a clear provenance signature is high. However, when a low HMC is paired with only durable minerals, for example, a high ZTR concentration (Hubert, 1962), then diagenetic dissolution over one or more sedimentary cycles has likely taken place (Garzanti, 2017). Morton (2012) highlights the presence of corrosion textures on grain surfaces (see also Andò et al., 2012), decreasing mineral diversity with increasing depth, and a relationship between permeability and mineral abundance as additional diagnosing factors for mineral dissolution. The relationship between reducing mineral diversity and increasing depth is connected by an increase in pore fluid temperatures and changes in fluid composition (Morton & Hallsworth, 2007). The depths at which minerals disappear varies for different regions, suggesting additional influence from other factors such as the individual geothermal gradient, fluid flow, and time (Morton & Hallsworth, 1999). The result of decreasing mineral diversity with increasing depth, attributed to burial diagenesis, has been observed within many basins worldwide. Examples where reduction in heavy-mineral diversity has been linked to diagenesis include Palaeocene-Eocene sandstones from the North Sea (Morton & Hallsworth, 2007), Plio-Pleistocene sandstones from the Gulf of Mexico (Milliken, 2007), Eocene-Oligocene sandstones from New Zealand (Smale, 2007) and post-Eocene successions from the Nile Delta (Garzanti et al., 2018). Thus reduction of heavy-mineral diversity, along with ZTR increase, needs to be considered for the ancient turbidite samples investigated here.

It has been suggested that the rate of dissolution is directly affected by the permeability of the rock by which the fluid is traveling, with a higher permeable rock resulting in greater fluid flow, and therefore, higher rates of dissolution (Morton & Hallsworth, 2007). Theoretically, diagenetic processes are primarily controlled by temperature, pressure, fluid chemistry, and time. During fluid-mineral interactions (e.g., mineral dissolution), fluid is passing through the rock, which in turn is directly controlled by rock porosity and permeability. Therefore, higher fluid flow, or greater time at a given fluid flow, should result in stronger diagenetic processes, that is, greater dissolution effects (Bjørlykke, 1994). Examples for this effect are seen within the Kura basin, where sandstones with low porosity and permeability, due to their volcanic provenance, cause unstable minerals to remain at greater depths compared to other basins globally (Morton et al., 2003). Blatt and Sutherland (1969) show preservation of diverse assemblages within siltstones and mudstones compared to adjacent sandstones, and Bramlette (1941) suggests cementation led to a reduction in porosity and permeability, meaning less stable minerals were more prevalent compared to their less cemented counterparts. However, it is worth mentioning that dissolution may also be prevalent in sedimentary rocks of low permeability, indicating that other factors can dominate this process (Garzanti et al., 2018; Limonta et al., 2023).

As mentioned in Section 5.2.1, both Strubach and Gamsbach locations have considerable heavy-mineral variations between base (A) and top (B) samples, originating from a single turbidite bed. These effects are regardless of grain-size fraction, and provenance changes between the basal and upper parts of single turbidite beds are not a probable cause. The sorting values of a lithified rock can give suggestions about its permeability and porosity, values for the “A” samples for both Strubach (0.55), and Gams (0.63) are greater than those for the “B” samples (0.48 and 0.411 respectively), although contrasts are moderate. Coarser, less sorted samples suggest less permeability and may subsequently reduce dissolution of less stable minerals such as apatite and garnet, which are plentiful within the “A” samples. This, and the higher diversity in the “A” samples could be a reflection of variations in fluid flow induced mineral dissolution. However, both samples were checked under the optical microscope for evidence of surface corrosion. For A and B samples, for both locations, no evidence of pitting or even any trace of corrosion could be found in the less stable minerals (i.e., apatite, staurolite, and garnet). Notably for apatite in SF-1-6A, the prismatic faces were completely intact. Therefore, we can rule out heavy-mineral dissolution during burial diagenesis as a control factor for these heavy-mineral assemblages and thus, as cause for the contrasts between “A” and “B” samples.

5.6. Hindered Settling

Briefly described in Section 2.1, hindered settling occurs when increased sediment concentration influences grain interactions, thus causing settling velocities to decrease. During turbidity currents, especially toward the base, sediment concentration is likely to be greater. Therefore, one can reasonably assume that the lower coarse beds (sample “A”) have derived from denser turbidity currents, implying a higher impact of hindered settling. When comparing flows of similar density, finer grains experience greater hindered settling than coarser grains (Baas et al., 2022; Richardson & Zaki, 1954). However, what does this mean for our samples where we have minerals of varying densities? Could hindered settling counteract density contrasts, causing size-density sorting to be less effective within these deposits?

After Richardson and Zaki (1954), hindered settling velocity ($w_{s,h}$) is defined as:

$$w_{s,h} = w_{s,0}(1 - C)^m \quad (5a)$$

where $w_{s,0}$ is the settling velocity, C is the volumetric suspended particle concentration, and m is the coefficient newly defined by Baas et al. (2022):

$$m = 5.037 - 2.839 \left(1 - e^{-0.1687 Re_p^{0.38}} \right) \quad (5b)$$

where Re_p is the particle Reynolds number:

$$Re_p = \frac{w_{s,0} D}{\nu} \quad (5c)$$

where D is the particle diameter and ν is the kinematic viscosity.

Considering hindered settling (Equation 5a), the settling velocity is relatively reduced by factor $(1 - C)^m$. Because $1 - C$ is <1 for any particle concentration, higher m leads to lower $(1 - C)^m$, in turn resulting in a stronger relative

reduction of the settling velocity. A higher m is given by decreasing Re_p (Equation 5b), which in turn decreases by decreasing $w_{s,0}$ (Equation 5c). Irrespective of using Stokes' Law or the formulation of Cheng (1997), at the same particle size, $w_{s,0}$ gets smaller by decreasing the density contrast between the settling particle and the medium. Thus, the settling velocity of less dense mineral grains is relatively more reduced by the hindered settling effect than the settling velocity of higher-density mineral grains. Consequently, an increase in the particle (sediment) concentration enhances the effect of hydrodynamic sorting. Considering a 63- μm -sized quartz (2.65 g/cm³) and magnetite (5.15 g/cm³) grain, the absolute settling velocity after Cheng (1997) is considerably reduced from 2.40 to 0.68 mm/s (71.6% reduction) for quartz and from 5.91 to 1.72 mm/s (70.9% reduction) for magnetite by the hindered settling effect at a sediment concentration of 23% (23% is the suggested maximum concentration a turbidity flow can reach; Lowe, 1982; Shanmugam, 2019). This relates to a corresponding relative difference in settling velocity reduction <1%. Thus, even at the extreme case of high sediment concentration and minerals of strong density contrast, the influence of the hindered settling effect on size-density sorting is rather minor. Together, the observed difference between base "A" and top "B" samples cannot be explained by (a) contrasting provenance (samples originate from the same turbidite bed), (b) hydrodynamic differences (particularly differences in ATi), (c) diagenetic modification, and (d) hindered settling; thus, a satisfying explanation for the observed deviation from the predicted mineral ratios remains open.

5.7. Implications for Sediment Provenance

Grain-size inheritance cannot be expected to provide distinct clues on specific source rocks like particular lithoclasts, mineral chemistry, or geochronology. However, some hints might be possible based on either (a) precise knowledge of the source rocks and their preferred grain-size range for specific minerals or (b) empirically based assumptions on general grain-size distribution of minerals in specific rocks or rock families. For instance, coarse-grained garnet in higher-grade metamorphic rocks (e.g., Krippner et al., 2015; Schönig et al., 2021) or fine-grained tourmaline in metapelitic rocks (von Eynatten & Dunkl, 2012). At a large scale, for example, the Denmark placer where the inheritance of coarse-grained garnet has been demonstrated, this may still hint to a crystalline hinterland composed of predominantly higher-grade metamorphic rocks (i.e., Scandinavia). The lack of coarse-grained tourmaline at Höflein and Strubach is well in line with rare granitoid sources and abundant low-grade metamorphics (Egger et al., 2002).

Epidote typically replaces plagioclase at greenschist to lower amphibolite facies conditions; in the case of mafic and metapelitic rocks, epidotes are typically small when compared to metagranitoid rocks. This is in line with the observation of inherited fine-grained epidote at Gamsbach, where upper greenschist to lower amphibolite facies metamorphic source rocks were inferred from heavy-mineral data and sandstone modal composition (Koukal et al., 2022).

Having highlighted the impact that grain-size inheritance may exert on sediments and their related heavy-mineral assemblages, it is important to attempt to mitigate its effect when using heavy-mineral analysis during provenance studies. Most striking is the difference in prevalent heavy minerals across one single turbidite bed. This especially emphasizes the importance of considering at which part of the succession samples are being collected. First, the simplest solution to this problem would be to take multiple samples from each sedimentary layer being studied, or in this specific case, each turbidite succession. This would allow for comparisons to be made within each bed, as was completed in this study, and for anomalous heavy-mineral grain sizes to be identified. Following on from this, these heavy minerals are to be used with caution when determining provenance signatures. In addition, if evidence of grain-size inheritance is identified, this can further aid in identifying source areas and facies conditions that are directly influencing mineral grain size.

One other important factor to consider during heavy-mineral analysis is the impact the grain-size fraction selected may have on the abundance of heavy minerals measured. It is clear from this study how important grain-size fraction selection is, and how much mineral diversity can vary from one fraction to another, in addition to the obvious presence of grain-size inheritance within certain grain-size fractions. This significance was mentioned in Stutenbecker et al. (2023) who looked at the temporal compositional variability of four smaller rivers in Germany. Finding the main cause of changing sediment composition over the year was due to grain-size distribution variations rather than changes in provenance signatures. They highlight the need to measure "several narrow grain sizes" to reduce the aforementioned variability, specifying the need to have the composition and texture of the source rock. This requirement can be reiterated here, as it is clear that source rock composition has a large impact

on the grain-size distribution of the minerals deposited. The grain-size fraction measured should be directly based on the grain-size distribution of the bulk sample and the particular methods being applied during heavy-mineral analysis, alongside knowledge of the effects of inherited grain size on size-density relations.

In detrital geochronology, fertility and grain-size bias in the age data, either crystallization or cooling ages, should be minimized (e.g., Lawrence et al., 2011; Malusa et al., 2016). To ensure consideration of the most representative grain-size ranges of the minerals to be dated, inheritance of mineral grain-size fractions from contrasting sources should be considered. One example of this is given in Augustsson et al. (2018), who highlight the importance of analyzing shape, roundness, and grain size versus age. They relate zircon ages to grain-size intervals, which aids in reducing both hydraulic and grain-size inheritance effects.

6. Conclusions

The importance of understanding the controls on a heavy-mineral composition, and the alterations it can undergo during erosion, transport, and deposition, is paramount for provenance studies. The impact of inherited grain-size distributions, which has been as yet largely neglected, was evaluated and quantified in this study using examples from both modern and ancient sediments. All samples were found to contain grain-size dependent variations that could not be explained by hydrodynamic size-density sorting alone.

Placer deposits, selected for the modern example due to their high-energy nature, are sediments expected to strictly follow hydrodynamic control, though modifications by re-entrainment sorting are known. However, even within these deposits, evidence of inherited grain size is obvious. When compared to the modeled, purely hydrodynamically controlled, heavy-mineral composition, a lack of fine-grained garnet is evident. In the turbidite deposits, grain-size inheritance is even more prevalent, with all samples containing affected heavy-mineral species. These include epidote enrichment in finer fractions, the lack of coarser-grained tourmaline, or the lack of finer-grained rutile, as compared to the hydrodynamic model. Alongside this, additional compositional differences were found between samples collected from the base or top of a single turbidite bed. These variations are further discussed considering effects of diagenesis or hindered settling, but both controls are concluded as unlikely causes.

Overall, the patterns observed within this study suggest grain-size inheritance is the rule rather than the exception. Many studies only consider the effect of hydrodynamics when using heavy-mineral distributions, or associate it as the overwhelming cause of size-dependent variability (e.g., Garzanti et al., 2008; Resentini et al., 2013). When attempting to model heavy-mineral compositions over the full grain-size range, inherited grain-size distributions may significantly affect the results. Therefore, it is of utmost importance to (a) understand the source regions and rock types where sediment may have originated and how grain-size inheritance may influence the sediments delivered and (b) apply analysis of several grain-size fractions so grain-size inheritance can be identified and mitigated and/or carefully select grain-size fractions based on bulk grain-size distributions.

Data Availability Statement

All data presented in this paper (heavy-mineral counts, grain-size distributions, and Raman spectroscopy spectra) is available at the Göttingen Research Online (GRO) online repository, it is cited under Feil (2023) GRO.data. <https://doi.org/10.25625/MVUIJQ>.

References

- Allen, J. R. (1982). *Sedimentary structures*. Elsevier.
- Andò, S., Bersani, D., Vignola, P., & Garzanti, E. (2009). Raman spectroscopy as an effective tool for high-resolution heavy-mineral analysis: Examples from major Himalayan and Alpine fluvio-deltaic systems. *Spectrochimica Acta Part A: Molecular and Biomolecular Spectroscopy*, 73(3), 450–455. <https://doi.org/10.1016/j.saa.2008.11.005>
- Andò, S., & Garzanti, E. (2014). Raman spectroscopy in heavy-mineral studies. *Geological Society, London, Special Publications*, 386(1), 395–412. <https://doi.org/10.1144/SP386.2>
- Andò, S., Garzanti, E., Padoan, M., & Limonta, M. (2012). Corrosion of heavy minerals during weathering and diagenesis: A catalog for optical analysis. *Sedimentary Geology*, 280, 165–178. <https://doi.org/10.1016/j.sedgeo.2012.03.023>
- Augustsson, C., Voigt, T., Bernhart, K., Kreißler, M., Gaupp, R., Gärtner, A., et al. (2018). Zircon size-age sorting and source-area effect: The German Triassic Buntsandstein Group. *Sedimentary Geology*, 375, 218–231. <https://doi.org/10.1016/j.sedgeo.2017.11.004>
- Baas, J. H., Baker, M. L., Buffon, P., Strachan, L. J., Bostock, H. C., Hodgson, D., et al. (2022). Blood, lead and spheres: A hindered settling equation for sedimentologists based on metadata analysis. *The Depositional Record*, 8(2), 603–615. <https://doi.org/10.1002/dep2.176>

Acknowledgments

Thanks to M. Wagreich, H. Egger (Vienna), A. Detamble, and A. Pekol (Gmunden) for helpful advice on turbidite sample locations in Austria and to Johannes Sucke for his preliminary research looking at hydrodynamic control of heavy-mineral assemblages on turbidites at the Höflein location in Austria. We appreciate careful reviews by Eduardo Garzanti and an anonymous reviewer as well as guest editor Chris Mark. Open Access funding enabled and organized by Projekt DEAL.

- Bagnold, R. A. (1954). Experiments on a gravity-free dispersion of large solid spheres in a Newtonian fluid under shear. *Proceedings of the Royal Society of London, Series A*, 225, 49–63. <https://doi.org/10.1098/rspa.1954.0186>
- Bjorlykke, K. (1994). Fluid-flow processes and diagenesis in sedimentary basins. *Geological Society, London, Special Publications*, 78(1), 127–140. <https://doi.org/10.1144/gsl.sp.1994.078.01.11>
- Blatt, H., & Sutherland, B. (1969). Intrastratal solution and non-opaque heavy minerals in shales. *Journal of Sedimentary Research*, 39(2), 591–600. <https://doi.org/10.1306/74D71CDA-2B21-11D7-8648000102C1865D>
- Bouma, A. H. (1962). *Sedimentology of some flysch deposits; a graphic approach to facies interpretation*. Elsevier.
- Bouma, A. H. (1964). Turbidites. *Developments in Sedimentology*, 3, 247–256. [https://doi.org/10.1016/S0070-4571\(08\)70967-1](https://doi.org/10.1016/S0070-4571(08)70967-1)
- Bramlette, M. N. (1941). The stability of minerals in Sandstone. *Journal of Sedimentary Research*, 11(1), 32–36. <https://doi.org/10.1306/D42690DA-2B26-11D7-8648000102C1865D>
- Briggs, L. I. (1965). Heavy mineral correlations and provenances. *Journal of Sedimentary Research*, 35(4), 939–955. <https://doi.org/10.1306/74D713B6-2B21-11D7-8648000102C1865D>
- Chaudhuri, A., Schönig, J., Pera, E. L., Eynatten, H. V., Chauhan, G., & Lünsdorf, N. K. (2023). Provenance changes revealed by a multi-proxy approach to sandstone analysis and its implications on palaeogeography: Mesozoic Kutch Basin, India. *Sedimentary Geology*, 452, 106411. <https://doi.org/10.1016/j.sedgeo.2023.106411>
- Cheng, N. S. (1997). Simplified settling velocity formula for sediment particle. *Journal of Hydraulic Engineering*, 123(2), 149–152. [https://doi.org/10.1061/\(ASCE\)0733-9429\(1997\)123:2\(149\)](https://doi.org/10.1061/(ASCE)0733-9429(1997)123:2(149))
- Clemmensen, L. B., Pye, K., Murray, A., & Heinemeier, J. (2001). Sedimentology, stratigraphy and landscape evolution of a Holocene coastal dune system, Lodbjerg, NW Jutland, Denmark. *Sedimentology*, 48(1), 3–27. <https://doi.org/10.1111/j.1365-3091.2001.00345.x>
- Dietz, V. (1973). Experiments on the influence of transport on shape and roundness of heavy minerals. *Contributions to Sedimentology*, 1, 103–125.
- Doody, J. P. (1991). *Sand dune inventory of Europe*. Joint Nature Conservation Committee/European Union for Coastal Conservation.
- Dunkl, I., von Eynatten, H., Andò, S., Lünsdorf, K., Morton, A., Alexander, B., et al. (2020). Comparability of heavy mineral data—The first interlaboratory round robin test. *Earth-Science Reviews*, 211, 103210. <https://doi.org/10.1016/j.earscirev.2020.103210>
- Egger, H. (2011). Stop A1/3 Strubach section. In *Climate and biota of the early Paleogene, field-trip guidebook, 5–8 June 2011, Salzburg, Austria* (pp. 37–38). Geological Survey of Austria.
- Egger, H., Homayoun, M., & Schnabel, W. (2002). Tectonic and climatic control of Paleogene sedimentation in the Rhenodanubian flysch basin (eastern Alps, Austria). *Sedimentary Geology*, 152(3–4), 247–262. [https://doi.org/10.1016/S0037-0738\(02\)00072-6](https://doi.org/10.1016/S0037-0738(02)00072-6)
- Egger, H., Rögl, F., & Wägrich, M. (2004). Biostratigraphy and facies of Paleogene deep-water deposits at Gams (Gosau group, Austria). In *Annalen des Naturhistorischen Museums in Wien. Serie A Für Mineralogie und Petrographie, Geologie und Paläontologie, Anthropologie Und Prähistorie* (Vol. 106, pp. 281–307).
- Feil, S. (2023). Supplementary dataset for the AGU publication ‘Inherited grain-size distributions’. *GRO.data*. <https://doi.org/10.25625/MVUIJQ>
- Fleet, W. F. (1926). Petrological notes on the old red sandstone of the west Midlands. *Geological Magazine*, 63(11), 505–516. <https://doi.org/10.1017/S0016756800085484>
- Folk, R. L., & Ward, W. C. (1957). Brazos River bar (Texas); a study in the significance of grain size parameters. *Journal of Sedimentary Research*, 27(1), 3–26. <https://doi.org/10.1306/74D70646-2B21-11D7-8648000102C1865D>
- Freise, F. W. (1931). Untersuchung von Mineralen auf Abnutzbarkeit bei Verfrachtung im Wasser. *Zeitschrift für Kristallographie, Mineralogie und Petrographie. Mitteilungen*, 41, 1–7. <https://doi.org/10.1007/BF02949762>
- Garnett, R. H., & Bassett, N. C. (2005). Placer deposits. In *Economic geology: One hundredth anniversary volume* (pp. 813–843). <https://doi.org/10.5382/AV100.25>
- Garzanti, E. (2017). The maturity myth in sedimentology and provenance analysis. *Journal of Sedimentary Research*, 87(4), 353–365. <https://doi.org/10.2110/jsr.2017.17>
- Garzanti, E., & Andò, S. (2019). Heavy minerals for junior woodchucks. *Minerals*, 9(3), 148. <https://doi.org/10.3390/min9030148>
- Garzanti, E., Andò, S., France-Lanord, C., Vezzoli, G., Censi, P., Galy, V., & Najman, Y. (2010). Mineralogical and chemical variability of fluvial sediments: 1. Bedload sand (Ganga–Brahmaputra, Bangladesh). *Earth and Planetary Science Letters*, 299(3–4), 368–381. <https://doi.org/10.1016/j.epsl.2010.09.017>
- Garzanti, E., Andò, S., Limonta, M., Fielding, L., & Najman, Y. (2018). Diagenetic control on mineralogical suites in sand, silt, and mud (Cenozoic Nile Delta): Implications for provenance reconstructions. *Earth-Science Reviews*, 185, 122–139. <https://doi.org/10.1016/j.earscirev.2018.05.010>
- Garzanti, E., Andò, S., & Vezzoli, G. (2008). Settling-equivalence of detrital minerals and grain-size dependence of sediment composition. *Earth and Planetary Science Letters*, 273(1–2), 138–151. <https://doi.org/10.1016/j.epsl.2008.06.020>
- Garzanti, E., Andò, S., & Vezzoli, G. (2009). Grain-size dependence of sediment composition and environmental bias in provenance studies. *Earth and Planetary Science Letters*, 277(3–4), 422–432. <https://doi.org/10.1016/j.epsl.2008.11.007>
- Garzanti, E., Andò, S., Vezzoli, G., Megid, A. A. A., & El Kammar, A. (2006). Petrology of Nile River sands (Ethiopia and Sudan): Sediment budgets and erosion patterns. *Earth and Planetary Science Letters*, 252(3–4), 327–341. <https://doi.org/10.1016/j.epsl.2006.10.001>
- Gazzi, P. (1965). On the heavy mineral zones in the geosyncline series; recent studies in the northern Apennines, Italy. *Journal of Sedimentary Research*, 35(1), 109–115. <https://doi.org/10.1306/74D71203-2B21-11D7-8648000102C1865D>
- Graham, D. J., & Midgley, N. G. (2000). Graphical representation of particle shape using triangular diagrams: An excel spreadsheet method. *Earth Surface Processes and Landforms*, 25(13), 1473–1477. [https://doi.org/10.1002/1096-9837\(200012\)25:13<1473::AID-ESP158>3.0.CO;2-C](https://doi.org/10.1002/1096-9837(200012)25:13<1473::AID-ESP158>3.0.CO;2-C)
- Harrell, J. A., & Eriksson, K. A. (1979). Empirical conversion equations for thin-section and sieve derived size distribution parameters. *Journal of Sedimentary Research*, 49(1), 273–280. <https://doi.org/10.1306/212F7711-2B24-11D7-8648000102C1865D>
- Hou, B., Keeling, J., & Van Gosen, B. S. (2017). Geological and exploration models of beach placer deposits, integrated from case-studies of Southern Australia. *Ore Geology Reviews*, 80, 437–459. <https://doi.org/10.1016/j.oregeorev.2016.07.016>
- Hounslow, M. W., & Morton, A. (2004). Evaluation of sediment provenance using magnetic mineral inclusions in clastic silicates: Comparison with heavy mineral analysis. *Sedimentary Geology*, 171(1–4), 13–36. <https://doi.org/10.1016/j.sedgeo.2004.05.008>
- Hubert, J. F. (1962). A zircon-tourmaline-rutile maturity index and the interdependence of the composition of heavy mineral assemblages with the gross composition and texture of sandstones. *Journal of Sedimentary Research*, 32(3), 440–450. <https://doi.org/10.1306/74D70CE5-2B21-11D7-8648000102C1865D>
- Hutton, C. O. (1950). Studies of heavy detrital minerals. *GSA Bulletin*, 61(7), 635–710. [https://doi.org/10.1130/0016-7606\(1950\)61\[635:SOHDM\]2.0.CO;2](https://doi.org/10.1130/0016-7606(1950)61[635:SOHDM]2.0.CO;2)
- Komar, P. D. (1985). The hydraulic interpretation of turbidites from their grain sizes and sedimentary structures. *Sedimentology*, 32(3), 395–407. <https://doi.org/10.1111/j.1365-3091.1985.tb00519.x>

- Komar, P. D. (1991). The hydraulic interpretation of turbidites from their grain sizes and sedimentary structures. In D. A. Stow (Ed.), *Deep-water turbidite systems* (pp. 41–53). <https://doi.org/10.1002/9781444304473.ch3>
- Komar, P. D. (2007). Chapter 1 the entrainment, transport and sorting of heavy minerals by waves and currents. In M. A. Mange & D. T. Wright (Eds.), *Heavy minerals in use. Developments in sedimentology* (Vol. 58, pp. 3–48). Elsevier. [https://doi.org/10.1016/S0070-4571\(07\)58001-5](https://doi.org/10.1016/S0070-4571(07)58001-5)
- Komar, P. D., & Wang, C. (1984). Processes of selective grain transport and the formation of placers on beaches. *The Journal of Geology*, 92(6), 637–655. <https://doi.org/10.1086/628903>
- Koukal, V., Wagreich, M., Kallanxhi, M. E., & Knierzinger, W. (2022). The Paleogene Gosau group slope basins of the incipient Eastern Alpine orogenic wedge: A case study at the Gams basin (Austria). *Minerals*, 12(2), 178. <https://doi.org/10.3390/min12020178>
- Krippner, A., Meinhold, G., Morton, A., Russell, E., & von Eynatten, H. (2015). Grain-size dependence of garnet composition revealed by provenance signatures of modern stream sediments from the western Hohe Tauern (Austria). *Sedimentary Geology*, 321, 25–38. <https://doi.org/10.1016/j.sedgeo.2015.03.002>
- Krippner, A., Meinhold, G., Morton, A., Schöning, J., & von Eynatten, H. (2016). Heavy minerals and garnet geochemistry of stream sediments and bedrocks from the Almklovdalen area, Western Gneiss Region, SW Norway: Implications for provenance analysis. *Sedimentary Geology*, 336, 96–105. <https://doi.org/10.1016/j.sedgeo.2015.09.009>
- Lawrence, R. L., Cox, R., Mapes, R. W., & Coleman, D. S. (2011). Hydrodynamic fractionation of zircon age populations. *GSA Bulletin*, 123(1–2), 295–305. <https://doi.org/10.1130/B30151.1>
- Limonta, M., Garzanti, E., & Resentini, A. (2023). Petrology of Bengal fan turbidites (IODP expeditions 353 and 354): Provenance versus diagenetic control. *Journal of Sedimentary Research*, 93(4), 256–272. <https://doi.org/10.2110/jsr.2022.071>
- Löffler, R. (2013). *Reservoir properties of glauconite sandstones (Greifenstein Formation) in the quarry Strombauamt (Unpublished master's thesis)*. Universität Wien.
- Lowe, D. R. (1982). Sediment gravity flows; II, Depositional models with special reference to the deposits of high-density turbidity currents. *Journal of Sedimentary Research*, 52(1), 279–297. <https://doi.org/10.1306/212F7F31-2B24-11D7-8648000102C1865D>
- Lünsdorf, N. K., Kalies, J., Ahlers, P., Dunkl, I., & von Eynatten, H. (2019). Semi-automated heavy-mineral analysis by Raman spectroscopy. *Minerals*, 9(7), 385. <https://doi.org/10.3390/min9070385>
- Lünsdorf, N. K., Lünsdorf, J. O., Újvári, G., Dunkl, I., Wolfram, L., Hobrecht, A., et al. (2023). From outcrop to spectrum—A fully automated approach to modal mineralogy of silt-sized sediment applied to Central European loess. *Journal of Geophysical Research: Earth Surface*, 128(12), e2023JF007364. <https://doi.org/10.1029/2023jf007364>
- Malusa, M. G., Resentini, A., & Garzanti, E. (2016). Hydraulic sorting and mineral fertility bias in detrital geochronology. *Gondwana Research*, 31, 1–19. <https://doi.org/10.1016/j.gr.2015.09.002>
- Mange, M., & Maurer, H. (1992). *Heavy minerals in color*. Chapman and Hall.
- Mange, M., & Wright, D. (2007). *Heavy minerals in use. Developments in sedimentology* (Vol. 58). Elsevier.
- Mange-Rajetzky, M. (1983). Sediment dispersal from source to shelf on an active continental margin, S. Turkey. *Marine Geology*, 52(1–2), 1–26. [https://doi.org/10.1016/0025-3227\(83\)90018-X](https://doi.org/10.1016/0025-3227(83)90018-X)
- McIntyre, D. D. (1959). The hydraulic equivalence and size distributions of some mineral grains from a beach. *The Journal of Geology*, 67(3), 278–301. <https://doi.org/10.1086/626584>
- Milliken, K. L. (2007). Chapter 8 provenance and diagenesis of heavy minerals, Cenozoic units of the Northwestern Gulf of Mexico sedimentary basin. In M. A. Mange & D. T. Wright (Eds.), *Heavy minerals in use. Developments in Sedimentology* (Vol. 58, pp. 247–261). Elsevier. [https://doi.org/10.1016/S0070-4571\(07\)58008-8](https://doi.org/10.1016/S0070-4571(07)58008-8)
- Morton, A. (1985). Heavy minerals in provenance studies. In G. G. Zuffa (Ed.), *Provenance of Arenites, NATO ASI series* (Vol. 148, pp. 249–277). Springer. https://doi.org/10.1007/978-94-017-2809-6_12
- Morton, A. (2012). Value of heavy minerals in sediments and sedimentary rocks for provenance, transport history and stratigraphic correlation. In P. Sylvester (Ed.), *Quantitative mineralogy and microanalysis of sediments and sedimentary rocks; mineralogical association of Canada short course series* (Vol. 42, pp. 133–165). Mineralogical Association of Canada.
- Morton, A., Allen, M., Simmons, M., Spathopoulos, F., Still, J., Hinds, D., et al. (2003). Provenance patterns in a neotectonic basin: Pliocene and Quaternary sediment supply to the South Caspian. *Basin Research*, 15(3), 321–337. <https://doi.org/10.1046/j.1365-2117.2003.00208.x>
- Morton, A., & Hallsworth, C. (1994). Identifying provenance-specific features of detrital heavy mineral assemblages in sandstones. *Sedimentary Geology*, 90(3–4), 241–256. [https://doi.org/10.1016/0037-0738\(94\)90041-8](https://doi.org/10.1016/0037-0738(94)90041-8)
- Morton, A., & Hallsworth, C. (1999). Processes controlling the composition of heavy mineral assemblages in sandstones. *Sedimentary Geology*, 124(1–4), 3–29. [https://doi.org/10.1016/S0037-0738\(98\)00118-3](https://doi.org/10.1016/S0037-0738(98)00118-3)
- Morton, A., & Hallsworth, C. (2007). Chapter 7 stability of detrital heavy minerals during burial diagenesis. In M. A. Mange & D. T. Wright (Eds.), *Heavy minerals in use. Developments in sedimentology* (Vol. 58, pp. 215–245). Elsevier. [https://doi.org/10.1016/S0070-4571\(07\)58007-6](https://doi.org/10.1016/S0070-4571(07)58007-6)
- Morton, A., & Hurst, A. (1995). Correlation of sandstones using heavy minerals: An example from the Statfjord formation of the Snorre field, northern North Sea. *Geological Society, London, Special Publications*, 89(1), 3–22. <https://doi.org/10.1144/GSL.SP.1995.089.01.02>
- Morton, A., & Johnsson, M. (1993). Factors influencing the composition of detrital heavy mineral suites in Holocene sands of the Apure River drainage basin, Venezuela. In M. J. Johnsson & A. Basu (Eds.), *Processes controlling the composition of clastic sediments* (Vol. 284, pp. 171–185). Geological Society of America.
- Morton, A., & Smale, D. (1990). The effects of transport and weathering on heavy minerals from the Cascade River, New Zealand. *Sedimentary Geology*, 68(1–2), 117–123. [https://doi.org/10.1016/0037-0738\(90\)90122-A](https://doi.org/10.1016/0037-0738(90)90122-A)
- Norman, T. N. (1969). A method to study the distribution of heavy-mineral grain abundance in a turbidite. *Sedimentology*, 13(3–4), 263–280. <https://doi.org/10.1111/j.1365-3091.1969.tb00173.x>
- Pyles, D. R., Straub, K. M., & Stammer, J. G. (2013). Spatial variations in the composition of turbidites due to hydrodynamic fractionation. *Geophysical Research Letters*, 40(15), 3919–3923. <https://doi.org/10.1002/grl.50767>
- R Core Team. (2021). *A language and environment for statistical computing*. R Foundation for Statistical Computing. Retrieved from <https://www.R-project.org/>
- Resentini, A., Malusà, M. G., & Garzanti, E. (2013). MinSORTING: An Excel® worksheet for modelling mineral grain-size distribution in sediments, with application to detrital geochronology and provenance studies. *Computers & Geosciences*, 59, 90–97. <https://doi.org/10.1016/j.cageo.2013.05.015>
- Richardson, J. F., & Zaki, W. N. (1954). The sedimentation of a suspension of uniform spheres under conditions of viscous flow. *Chemical Engineering Science*, 3(2), 65–73. [https://doi.org/10.1016/0009-2509\(54\)85015-9](https://doi.org/10.1016/0009-2509(54)85015-9)
- Rittenhouse, G. (1943). Transportation and deposition of heavy mineral. *GSA Bulletin*, 54(12), 1725–1780. <https://doi.org/10.1130/GSAB-54-1725>
- RStudio Team. (2022). *RStudio: Integrated development environment for R*. RStudio, PBC. Retrieved from <https://posit.co>

- Rubey, W. W. (1933a). The size distribution of heavy minerals within a water-laid sandstone. *Journal of Sedimentary Research*, 3(1), 3–29. <https://doi.org/10.1306/D4268E37-2B26-11D7-8648000102C1865D>
- Rubey, W. W. (1933b). Settling velocity of gravel, sand, and silt particles. *American Journal of Science*, s5–25(148), 325–338. <https://doi.org/10.2475/ajs.s5-25.148.325>
- Savage, K. M., de Cesero, P., & Potter, P. E. (1988). Mineralogic maturity of modern sand along a high-energy tropical coast: Baixada de Jacarepaguá, Rio de Janeiro, Brazil. *Journal of South American Earth Sciences*, 1(4), 317–328. [https://doi.org/10.1016/0895-9811\(88\)90020-X](https://doi.org/10.1016/0895-9811(88)90020-X)
- Schönig, J., Benner, C., Meinhold, G., von Eynatten, H., & Lünsdorf, N. (2023). Detrital garnet petrology challenges Paleoproterozoic ultrahigh-pressure metamorphism in western Greenland. *European Journal of Mineralogy*, 35(4), 479–498. <https://doi.org/10.5194/ejm-35-479-2023>
- Schönig, J., von Eynatten, H., Meinhold, G., & Lünsdorf, N. K. (2021). Life-cycle analysis of coesite-bearing garnet. *Geological Magazine*, 158(8), 1421–1440. <https://doi.org/10.1017/S0016756821000017>
- Shanmugam, G. (2019). Slides, slumps, debris flows, turbidity currents, hyperpycnal flows, and bottom currents. In J. H. Steel, S. A. Thorpe, & K. K. Turekian (Eds.), *Ocean currents* (pp. 228–257). Academic Press.
- Slingerland, R. L. (1977). The effects of entrainment on the hydraulic equivalence relationships of light and heavy minerals in sands. *Journal of Sedimentary Research*, 47(2), 753–770. <https://doi.org/10.1306/212F7243-2B24-11D7-8648000102C1865D>
- Slingerland, R. L. (1984). Role of hydraulic sorting in the origin of fluvial placers. *Journal of Sedimentary Research*, 54(1), 137–150. <https://doi.org/10.1306/212F83C8-2B24-11D7-8648000102C1865D>
- Slingerland, R. L., & Smith, N. D. (1986). Occurrence and formation of water-laid placers. *Annual Review of Earth and Planetary Sciences*, 14(1), 113–147. <https://doi.org/10.1146/annurev.ea.14.050186.000553>
- Smale, D. (2007). Chapter 22 sediment trails in tectonically active Islands: Heavy minerals in use in New Zealand. In M. A. Mange & D. T. Wright (Eds.), *Heavy minerals in use. Developments in sedimentology* (Vol. 58, pp. 569–585). Elsevier. [https://doi.org/10.1016/S0070-4571\(07\)58022-2](https://doi.org/10.1016/S0070-4571(07)58022-2)
- Stutenbecker, L., Scheuevens, D., Hinderer, M., Hornung, J., Petschick, R., Raila, N., & Schwind, E. (2023). Temporal variability of fluvial sand composition: An annual time series from four rivers in SW Germany. *Journal of Geophysical Research: Earth Surface*, 128(6), e2023JF007138. <https://doi.org/10.1029/2023JF007138>
- Talling, P. J., Masson, D. G., Sumner, E. J., & Malgesini, G. (2012). Subaqueous sediment density flows: Depositional processes and deposit types. *Sedimentology*, 59(7), 1937–2003. <https://doi.org/10.1111/j.1365-3091.2012.01353.x>
- Thiel, G. (1945). Mechanical effects of stream transportation in mineral grains of sand size. *GSA Bulletin*, 56, 1207.
- Turner, G., & Morton, A. (2007). Chapter 14 the effects of burial diagenesis on detrital heavy mineral grain surface textures. In M. A. Mange & D. T. Wright (Eds.), *Heavy minerals in use. Developments in Sedimentology* (Vol. 58, pp. 393–412). Elsevier. [https://doi.org/10.1016/S0070-4571\(07\)58014-3](https://doi.org/10.1016/S0070-4571(07)58014-3)
- Udden, J. A. (1914). Mechanical composition of clastic sediments. *GSA Bulletin*, 25(1), 655–744. <https://doi.org/10.1130/GSAB-25-655>
- van Andel, T. H. (1950). *Provenance, transport and deposition of rhine sediments: A heavy mineral study*. Veenman.
- van Andel, T. H. (1959). Reflections on the interpretation of heavy mineral analyses. *SEPM Journal of Sedimentary Research*, 29(2), 153–163. <https://doi.org/10.1306/74D708B7-2B21-11D7-8648000102C1865D>
- van Tassel, J. (1981). Silver Abyssal plain carbonate turbidite: Flow characteristics. *The Journal of Geology*, 89(3), 317–333. <https://doi.org/10.1086/628594>
- Velbel, M. A. (2007). Chapter 4 surface textures and dissolution processes of heavy minerals in the sedimentary cycle: Examples from pyroxenes and amphiboles. In M. A. Mange & D. T. Wright (Eds.), *Heavy minerals in use. Developments in Sedimentology* (Vol. 58, pp. 113–150). Elsevier. [https://doi.org/10.1016/S0070-4571\(07\)58004-0](https://doi.org/10.1016/S0070-4571(07)58004-0)
- Viator, D. (2003). *Detrital tourmaline as an indicator of provenance: A chemical and sedimentological study of modern sands from the black hills, South Dakota* (p. 1520). Louisiana State University (Baton Rouge) Master's Theses.
- von Eynatten, H., & Dunkl, I. (2012). Assessing the sediment factory: The role of single grain analysis. *Earth-Science Reviews*, 115(1–2), 97–120. <https://doi.org/10.1016/j.earscirev.2012.08.001>
- Walker, R. G. (1965). The origin and significance of the internal sedimentary structures of turbidites. *Proceedings of the Yorkshire Geological Society*, 35(1), 1–32. <https://doi.org/10.1144/pygs.35.1.1>
- Weltje, G. J., & von Eynatten, H. (2004). Quantitative provenance analysis of sediments: Review and outlook. *Sedimentary Geology*, 171(1–4), 1–11. <https://doi.org/10.1016/j.sedgeo.2004.05.007>
- Whitney, D. L., & Evans, B. W. (2010). Abbreviations for names of rock-forming minerals. *American Mineralogist*, 95(1), 158–187. <https://doi.org/10.2138/am.2010.3371>
- Zimmermann, S., Mark, C., Chew, D., & Voice, P. J. (2018). Maximising data and precision from detrital zircon U-Pb analysis by LA-ICPMS: The use of core-rim ages and the single-analysis Concordia age. *Sedimentary Geology*, 375, 5–13. <https://doi.org/10.1016/j.sedgeo.2017.12.020>